W. S. Aiken Jr.

CONFIDENTIAL

Copy
RM L56E21a

414

NACA RM L56E21a

NACA

RESEARCH MEMORANDUM

LIFT-CURVE SLOPES DETERMINED IN FLIGHT ON A FLEXIBLE SWEPT-WING JET BOMBER

By William S. Aiken, Jr., and Raymond A. Fisher

Langley Aeronautical Laboratory
Langley Field, Va.

CLASSIFICATION CHANGED TO UNCLASSIFIED
AUTHORITY: NACA RESEARCH ABSTRACT NO. 12
EFFECTIVE DATE: SEPTEMBER 13, 1957 WE

CLASSIFIED DOCUMENT

NATIONAL ADVISORY COMMITTEE
FOR AERONAUTICS

WASHINGTON

December 19, 1956

60

CONFIDENTIAL

NATIONAL ADVISORY COMMITTEE FOR AERONAUTICS

RESEARCH MEMORANDUM

LIFT-CURVE SLOPES DETERMINED IN FLIGHT ON A FLEXIBLE SWEPT-WING JET BOMBER

By William S. Aiken, Jr., and Raymond A. Fisher

SUMMARY

An analysis is made of the effects of Mach number and dynamic pressure on the lift-curve slope of a large flexible swept-wing jet-propelled airplane by using flight measurements of normal acceleration and angle of attack with auxiliary instrumentation as needed. The methods and procedures used to correct the flight measurements (obtained in abrupt push-pull maneuvers) and to convert the flight test data to equivalent rigid conditions for comparison with rigid-model wind-tunnel tests are described in detail. The airplane angle of zero lift and the airplane-less-tail angle of zero lift for the Mach number range of the flight tests (0.42 to 0.81) are also presented. Excellent agreement was obtained in the comparison between flight and wind-tunnel rigid lift-curve slopes and angles of zero lift.

INTRODUCTION

The lift-curve slope and the effects of wing flexibility on the lift-curve slope are important factors in the design of present-day aircraft. Generally, design values of lift-curve slope are based on rigid-model wind-tunnel results and theoretical methods for estimating the effects of flexibility on wing-load distributions and thereby on airplane lift-curve slope. Actually, little information exists where these design procedures have been verified experimentally. As a result of an extensive flight investigation carried out by the National Advisory Committee for Aeronautics with a large flexible bomber airplane sufficient lift-curve-slope data were obtained over a fairly wide range of Mach number and dynamic pressure in quasi-static maneuvers to attempt an analysis. Some preliminary values of rigid-airplane lift-curve slope estimated from flexible-airplane flight test values obtained at one altitude have been previously presented in reference 1.

A principal objective of the present report is to show the comparison of rigid-airplane lift-curve slopes derived from flexible-airplane flight

test values with values of rigid lift-curve slope obtained from wind-tunnel tests. An equally important objective is the development of a rational method for obtaining rigid lift-curve slopes from flexible flight test values. This rational method is essentially the reverse of standard procedures used in design for estimating the effects of flexibility on airplane lift-curve slope. The report is organized to show the step-by-step analysis procedure followed from raw data to the final rigid lift-curve-slope variation with Mach number. The more or less standard corrections to angle of attack and airplane-normal-force-coefficient measurements are described in detail and a method for accounting for recorder lag necessary for the present analysis is given. In addition, angles of zero lift determined from the flight tests are correlated and compared with wind-tunnel results.

SYMBOLS

A,B	defined by equation (22)
AR	aspect ratio
c_{l_α}	two-dimensional lift-curve slope, per degree
C_{N_A}	airplane normal-force coefficient
$C_{N_{A_C}}$	airplane normal-force coefficient corrected for pitching-acceleration tail load and defined by equation (A13)
$\dot{C}_{N_{A_C}}$	time derivative of $C_{N_{A_C}}$
$C_{N_{A_{trim}}}$	airplane normal-force coefficient for trim in level flight
$\Delta C_{N_{add}}$	incremental wing-fuselage normal-force coefficient due to additional type of loads, includes wing flexibility effects
ΔC_{N_i}	incremental wing-fuselage normal-force coefficient due to wing inertia flexibility effects
ΔC_{N_R}	incremental wing-fuselage normal-force coefficient for rigid wing case
ΔC_{N_T}	incremental total wing-fuselage normal-force coefficient, includes wing flexibility effects

$K_1 = \left(\frac{\partial C_N}{\partial \alpha}\right)_{tail}\left(1 - \frac{d\epsilon}{d\alpha}\right)\frac{S_t}{S}$

$\Delta C_{N_{\ddot{\theta}}}$ defined by equation (A12)

$K_2 = \left(\frac{\partial C_N}{\partial \alpha}\right)_{tail}\frac{d\epsilon}{d\alpha}\frac{S_t}{S}$

$K_3 = \left(\frac{\partial C_N}{\partial \delta}\right)_{tail}\frac{S_t}{S}$

L_T tail load, lb

M Mach number

S wing area, sq ft

S_t tail area, sq ft

V true airspeed, ft/sec

W airplane weight, lb

a_m slope of measured airplane normal-force coefficient ($\ddot{\theta} = 0$) against angle of attack, per deg

a_F faired slope of flexible tail-on normal-force coefficient against angle of attack, per deg

m_{add} calculated slope of additional flexible wing-fuselage normal-force coefficient against angle of attack, per deg

m_f measured or calculated slope of flexible tail-off normal-force coefficient against angle of attack, per deg

m_F faired slope of flexible tail-off normal-force coefficient against angle of attack, per deg

m_R slope of rigid tail-off normal-force coefficient against angle of attack, per deg

m_{R_w} weighted mean values of m_R, per deg

n_{boom} normal load factor at angle-of-attack vane, g units

n_m measured normal load factor at accelerometer location, g units

n_{cg} normal load factor at airplane center of gravity, g units

Δn incremental load factor, g units

q dynamic pressure, lb/sq ft

r boom radius or approximate radius of fuselage nose, in.

t time, sec

w weighting factor

x distance of angle-of-attack vane forward of nose, in.

x_v distance of angle-of-attack vane from airplane center of gravity, ft

y distance of vane from boom center line, in.

α angle of attack, deg

α_1 angle of attack measured with respect to fuselage reference axis, deg

α_2 apparent true angle of attack with respect to fuselage reference axis, uncorrected for recorder lag, deg

α_3 true angle of attack with respect to fuselage reference axis, corrected for recorder lag, deg

α_{trim} true corrected angle of attack for trim in level flight, deg

α_w wing angle of attack with respect to free air stream, deg

$\Delta\alpha_{l_a}$ increment in measured angle of attack due to bending of boom under aerodynamic load, deg

$\Delta\alpha_{l_i}$ increment in measured angle of attack due to inertia bending of boom, deg

$\Delta\alpha_{l_{\dot{\theta}}}$ increment in measured angle of attack due to pitching velocity, deg

$\Delta\alpha_R$ increment in wing root angle of attack, deg

α_o	angle of zero lift (airplane tail-on)
α_{o_C}	angle of zero lift (airplane tail-on) determined from equations of form of equation (26), deg
$\alpha_{o_{WB}}$	angle of zero lift (airplane tail-off) determined from equations of form of equation (29), deg
$\alpha_{o_{adj}}$	angle of zero lift (airplane tail-on) defined in equation (30), deg
$\dot{\alpha}_3$	time rate of change of true corrected angle of attack, deg/sec
δ_{trim}	average root elevator angle for trim in level flight, deg
μ_{boom}	upwash at vane due to boom
$\mu_{fuselage}$	upwash at vane due to fuselage
μ_{wing}	upwash at vane due to wing
Λ	sweep angle of wing quarter-chord line, deg
τ	ratio of distance of angle-of-attack vane from wing 25-percent-chord location at center line to wing semispan
$\dot{\theta}$	airplane pitching velocity, radian/sec
$\ddot{\theta}$	airplane pitching acceleration, radian/sec^2
$\frac{d\epsilon}{d\alpha}$	downwash factor
$\left(\frac{\partial C_N}{\partial \alpha}\right)_{tail}$	tail lift-curve slope in terms of tail angle of attack, per deg
$\left(\frac{\partial C_N}{\partial \delta}\right)_{tail}$	tail lift-curve slope in terms of root elevator angle, per deg
$f(qm_R)$	defined by equation (15)

Bar over a symbol indicates geometric mean value.

APPARATUS AND TESTS

Airplane

The airplane used for this investigation was a six-engine, swept-wing, jet-propelled medium bomber. A photograph of the test airplane is shown in figure 1, and pertinent characteristics and dimensions used in this report are given in table I.

Instrumentation

The data used in the reduction and analysis given in the present paper were obtained from standard NACA recording instruments.

Normal accelerations were measured by both a single-component and a three-component air-damped accelerometer. Angular velocities and accelerations in pitch were measured by a rate-gyro-type, electrically differentiating, magnetically damped turnmeter. The angle of attack was measured by a flow-direction vane mounted on an NACA pitot-static head. The head was attached to a boom alined with the longitudinal axis of the airplane and was located approximately one fuselage diameter ahead of the original nose. The installation is shown in figure 2.

The recorded data were synchronized at 0.1-second intervals by means of a common timing circuit. All instruments were damped to about 0.67 of critical damping. A summary of quantities measured, instrument locations, and accuracies is given in the following table:

Quantity measured	Measurement station	Instrument range	Instrument accuracy
Normal acceleration, g units -			
Single component	34.2 percent M.A.C.	0 to 2	0.005
Three component	34.2 percent M.A.C.	-1 to 4	0.0125
Pitching velocity, radians/sec	25 percent M.A.C.	±0.25	0.005
Pitching acceleration, radians/sec^2	25 percent M.A.C.	±0.50	0.010
Angle of attack, deg	117 in. ahead of original nose	±30	0.10
Dynamic pressure, lb/sq ft	140 in. ahead of original nose	0 to 800	1.00
Static pressure, lb/sq ft	132 in. ahead of original nose	0 to 2,200	2.00
Time, sec	----------	----------	Approx. 0.005

Tests

All tests were made with the airplane in the clean condition. The flight data evaluated were taken from 68 push-down pull-up maneuvers made at pressure altitudes of approximately 20,000, 25,000, 30,000, and 35,000 feet and an overall Mach number range of 0.427 to 0.812. The tests were made at forward and normal center-of-gravity positions and airplane weights ranging from 107,000 to 127,000 pounds. Table II is a summary of the flight conditions for these runs. In the table are listed the flight and run numbers, average Mach number, average dynamic pressure, test altitude, weight, and center-of-gravity position. The Mach number and dynamic-pressure changes during any test run are indicated in the appropriate columns of table II.

METHODS AND RESULTS

The data-reduction and analysis procedures for determining the airplane lift-curve slope from quasi-static maneuvers in flight and for converting these results to rigid wing values for comparison with wind-tunnel data are somewhat complicated. Thus, the following sections present in detail:

(a) The corrections to the basic flight measurements of angle of attack and normal acceleration for the determination of airplane lift-curve slope

(b) A method of determining the lift-curve slope when lag is present in the angle-of-attack recording system

(c) The values of lift-curve slope for the test airplane for the 68 test maneuvers used in the analysis

(d) A method for determining values of tail-off lift-curve slope for the rigid airplane from flight test values

(e) A comparison of rigid airplane lift-curve slopes and rigid model wind-tunnel data

(f) The determination of the tail-off angle of zero lift

Basic Data

The basic data required for the present analysis are time histories of angle of attack and of airplane normal-force coefficient. In the appendix, the method of correcting the measured angle of attack to account

for upwash, pitching velocity, and boom deflections are given in detail along with the corrections applied to normal-force coefficient to account for the effects of pitching acceleration. The corrected angle of attack used in the analysis is given for the particular angle-of-attack measurement installation of the present tests by equation (A8) of the appendix as

$$\alpha_2 = 0.91\alpha_1 - 0.11 + 3034\frac{\dot{\theta}}{V} + 0.322\left(n_m - 1\right) + 0.593\ddot{\theta} \qquad (1)$$

and the airplane normal-force coefficient corrected for instrument location and out-of-trim tail load is given by equation (A13) of the appendix as

$$C_{N_{A_C}} = \frac{n_m W}{qS} + \frac{0.402W}{qS}\left(0.342 - \frac{c.g.}{100}\right)\ddot{\theta} + \frac{19.61}{q}\ddot{\theta} \qquad (2)$$

Normally, if the foregoing corrections have been made to the measured angles of attack (eq. (1)) and measured normal-force coefficients (eq. (2)) and if the lift-curve slope is constant over the angle-of-attack range considered, the following equation may be used to express the linear relationship between the normal-force coefficient at the center of gravity and the airplane angle of attack:

$$C_{N_{A_C}} = a_m(\alpha - \alpha_o) \qquad (3)$$

Time histories of $C_{N_{A_C}}$ and measured α_2 are shown in figures 3 and 4 by the square symbols for two typical push-pull maneuvers at a pressure altitude of approximately 35,000 feet. The flight conditions existing during these maneuvers are listed in table II. Also shown in time history form in figures 3 and 4 by circular symbols are the measured load factor at fuselage station 638 (34.2 percent of the wing M.A.C.), the pitching velocity $\dot{\theta}$, the pitching acceleration $\ddot{\theta}$, and the measured angle of attack α_1. A shift or time lag exists between $C_{N_{A_C}}$ and α_2 which is illustrated more clearly in figures 5 and 6 where plots of $C_{N_{A_C}}$ against α_2 seem to show nonlinear variations of normal force with airplane angle of attack.

Determination of lift-curve slopes with lag present in the angle-of-attack recording system.- The nonlinearities which appear in figures 5 and 6 indicate that all corrections necessary to determine lift-curve slope have not been applied. These nonlinearities were traced to lag in the recording Autosyn of the angle-of-attack measuring system. Although this recording instrument had a high enough natural frequency

(10 cps) for recording accurately most pitching maneuvers possible with the test airplane, it was thought that leakage of oil into the bearings of the Autosyn receiver unit at low temperatures changed the damping characteristics of the recorder so that a time lag was introduced. The lag was not determinable through calibrations or experiment since the amount of oil in the bearing and temperature of the unit could not be determined for the flight test conditions. Limited data obtained in tests subsequent to those reported here showed a linear variation of $C_{N_{A_C}}$ with α_2. Since these maneuvers were as abrupt as any reported herein, this precluded dynamic response of wings or fuselage as the cause of the lag loops described in the present paper.

Analysis of a large portion of the data used for the present report indicated that the angle of attack corrected for lag α_3 could be represented by the following equation:

$$\alpha_3 = \alpha_2 + \frac{d\alpha_3}{dt}(\text{Lag}) \tag{4}$$

A procedure was therefore adopted which would permit the evaluation of lift-curve slope a_m and angle of zero lift α_o without directly determining either $\frac{d\alpha_3}{dt}$ or the lag. The time derivative of the correct angle of attack $\frac{d\alpha_3}{dt}$ is still unknown but it is by definition proportional to $C_{\dot{N}_{A_C}}$ so that equation (4) may be rewritten as

$$\alpha_3 = \alpha_2 + \frac{(\text{Lag})}{a_m} C_{\dot{N}_{A_C}} \tag{5}$$

Substituting equation (5) into equation (3) makes it possible to determine the lift-curve slope and angle of zero lift (α_o) from readings of α_2 where lag effects are suspected as

$$\alpha_2 = \frac{1}{a_m} C_{N_{A_C}} + \alpha_o - \frac{(\text{Lag})}{a_m} C_{\dot{N}_{A_C}} \tag{6a}$$

With equations of the form of (6a), the flight data may be least squared to determine values of the coefficients $\frac{1}{a_m}$, α_o, and $\frac{(\text{Lag})}{a_m}$ with the measurement errors associated with the angle of attack α_2.

Results for two specific maneuvers.- The coefficients resulting from least-squares solutions for the two sample maneuvers (figs. 3 and 4)

using equation (6a) are given in the following table. For comparison purposes to indicate the improvement in fit, the coefficients were also calculated without the lag term from

$$\alpha_2 = \frac{1}{a_m} C_{N_{A_C}} + \alpha_o \qquad (6b)$$

which is, of course, an equation normally used for cases where there is no lag. The table also contains the standard errors of the coefficients, the number of test points used in the solutions, and the standard errors of estimate s:

Flight	Run	Figure	Number of points used	Type solution	$\frac{1}{a_m}$, deg	α_o, deg	$\frac{Lag}{a_m}$, deg-sec	Standard error, s, deg
9	1	3,5	30	Equation (6b)	10.54 ± 0.48	-2.35 ± 0.27	----------	±0.49
				Equation (6a)	11.16 ± 0.12	-2.60 ± 0.07	-1.42 ± 0.07	±.12
12	6	4,6	27	Equation (6b)	11.26 ± 0.31	-2.67 ± 0.18	----------	±0.30
				Equation (6a)	11.78 ± 0.11	-2.89 ± 0.06	-0.76 ± 0.05	±.10

The angles of attack as computed from the coefficients given in the preceding table for both sample maneuvers are shown in time history form in figures 3 and 4. The points are labeled with the equation number (6b) or (6a) from which they were calculated. The calculations made using the coefficients of equation (6a) are seen to approximate closely the time history of the angle of attack α_2. In figures 5 and 6, airplane normal-force coefficients are plotted as a function of the angle of attack corrected for lag α_3 (eq. (5)). Also shown in figures 5 and 6 are the lift curves determined from the $\frac{1}{a_m}$ and α_o coefficients using equation (6a).

The significant improvement in fitting the data with the inclusion of a lag parameter may thus be seen by reference to figures 3 and 4 where the time histories of α_2 are successfully duplicated, to figures 5 and 6 where the normal-force curves are linearized by the use of α_3, and to the previously presented table of results where the standard errors of estimate show a considerable decrease with the inclusion of a lag parameter.

The $\frac{1}{a_m}$ coefficients for the two representative runs are seen to be in reasonable agreement. Lift-curve slopes a_m obtained from the

solutions of equation (6a) would be 0.0896 for flight 9, run 1 and 0.0849 for flight 12, run 6.

The values of the angle of zero lift α_o listed in the table are thought to vary from run to run due to center-of-gravity, Mach number, and dynamic-pressure effects. For the two cases given, the standard errors of estimate s of $\pm 0.12^\circ$ and $\pm 0.10^\circ$ are considered to be acceptable since the basic reading accuracy for the angle-of-attack recorder is estimated to be $\pm 0.1^\circ$.

Lift-Curve Slope Variation With Mach Number and Dynamic Pressure

After establishing the method for correcting for the lag due to instrument characteristics, all 68 push-pull maneuvers were analyzed by using equation (6a) to determine both the airplane lift-curve slope and the angle of zero lift. The results of these computations are listed in table III with identifying run numbers, number of points used, standard errors of fit s, and average values of M and q. The runs are listed according to the approximate altitude and by increasing Mach numbers. The lag coefficients are not included since this was a byproduct necessary only to obtain the results.

The standard errors listed in table III are, with a few exceptions, considered to be acceptable since as was previously stated the estimated measuring accuracy for angle of attack was $\pm 0.10^\circ$.

The values of a_m listed in table III are shown plotted in figure 7 as a function of Mach number. In figure 7 different test-point symbols are used to differentiate the approximate altitude groupings of 20,000, 25,000, 30,000, and 35,000 feet. It was seen that considerable scatter existed in these data even for any particular altitude; however, two general trends may be noted: (1) There is the expected increase in lift-curve slope with increasing Mach number and (2) with increasing dynamic pressure for constant Mach number, the lift-curve slope decreases.

Conversion of flight data to rigid wing-fuselage values.- In order to determine lift-curve slopes for the rigid wing-fuselage combination for comparison with similar wind-tunnel data, it was first necessary to correct the flight tail-on lift-curve slopes to tail-off conditions by the use of the following equation:

$$m_f = a_m - \frac{\Delta L_T}{qS\,\Delta\alpha_3} \tag{7}$$

The tail loads were measured for the maneuvers considered here. The values of m_f from equation (7) are plotted in figure 8 and, at the high values of Mach numbers for any given altitude, the scatter is somewhat less than the scatter for the tail-on values of a_m given in figure 7.

The next step in the procedure is to establish the equations necessary for converting the flexible lift-curve slopes to equivalent rigid conditions. These equations are the same equations as would be used for calculating flexible results from rigid data. The incremental lift on a flexible wing surface may be expressed in coefficient form as

$$\Delta C_{N_T} = \Delta C_{N_{add}} + \Delta C_{N_i} \tag{8}$$

where ΔC_{N_T} is the incremental total wing-fuselage normal-force coefficient including aerodynamic and inertia flexibility effects, $\Delta C_{N_{add}}$ is the incremental wing-fuselage normal-force coefficient due to additional type of aerodynamic loads including wing flexibility effects, and ΔC_{N_i} is the incremental wing-fuselage normal-force coefficient due to wing inertia flexibility effects. Equation (8) may be rewritten as

$$\Delta C_{N_T} = \Delta C_{N_R} \frac{\Delta C_{N_{add}}}{\Delta C_{N_R}} + \frac{\partial C_{N_T}}{\partial n} \Delta n \tag{9}$$

Taking the derivative of equation (9) with respect to the root or rigid angle of attack leads to

$$m_f = m_R \frac{m_{add}}{m_R} + m_R \frac{\partial C_{N_T}/m_R}{\partial n} \frac{dn}{d\alpha_R} \tag{10}$$

In order to determine the inertia effect, the simplifying assumption is made that the normal acceleration across the wing span is constant and that

$$n \approx C_{N_A} q \frac{S}{W} \tag{11}$$

With this assumption, equation (10) becomes

$$m_f = m_R \frac{m_{add}}{m_R} + m_f m_R \frac{qS}{W} \frac{\partial C_{N_T}/m_R}{\partial n} \tag{12}$$

or

$$m_f = \frac{m_R \frac{m_{add}}{m_R}}{1 - qm_R \frac{S}{W} \frac{\partial C_{N_T}/m_R}{\partial n}} \tag{13}$$

Thus, in order to calculate the flexible wing or wing-fuselage lift-curve slope, the following parameters are required:

(a) m_R to be obtained from theory or experiment

(b) $\frac{m_{add}}{m_R}$ to be obtained from theory

(c) $\frac{\partial C_{N_T}/m_R}{\partial n}$ to be obtained from theory

(d) $\frac{qS}{W}$ to be specified for flight conditions

The values of $\frac{m_{add}}{m_R}$ and $\frac{\partial C_{N_T}/m_r}{\partial n}$ were obtained by use of the superposition method of reference 2 with some modifications. The modifications, in brief, consisted of using matrix procedures to determine aerodynamic and structural influence coefficients and the use of least-squares procedures in the determination of the equations necessary for establishing the angle-of-attack distributions across the wing as a function of span position and qm_R, the basic flexibility parameter. Fuselage effects were included in the calculations by the use of an overvelocity matrix determined using the method of reference 3. The parameters $\frac{m_{add}}{m_R}$ and $\frac{\partial C_{N_T}/m_R}{\partial n}$ were calculated for qm_R values of 0, 1, 5, 10, 15, 20, 25, 30, 35, 40, 45, and 50 $\frac{lb}{ft^2} \frac{1}{deg}$ and are shown in figures 9 and 10 as functions of qm_R. Also shown in these figures are similar curves from reference 4 which were used in the design of a later version of the test airplane. The differences between the two results are thought to be attributable mainly to the wing bending-stiffness distributions (EI) used in the two cases although they may be partly due to differences in values of two-dimensional lift-curve slopes used in each case. The NACA calculations used an EI distribution which resulted in calculated structural influence coefficients which closely checked those measured and reported in reference 5.

Equation (13) and the derived curves of $\frac{m_{add}}{m_R}$ (fig. 9) and $\frac{\partial C_{N_T}/m_R}{\partial n}$ (fig. 10) may now be used to estimate the lift-curve slope for the rigid

airplane from measurements of flexible lift-curve slopes made at various Mach numbers and dynamic pressures. Since the gross weights of the airplane varied only a maximum of 10 percent from the average gross weight of 116,000 pounds, equation (13) may be written as

$$m_f = \frac{m_R \frac{m_{add}}{m_R}}{1 - \frac{qm_R}{81.65} \frac{\partial C_{N_T}/m_R}{\partial n}} \tag{14}$$

Curves of m_f plotted against m_R may now be drawn as in figure 11 for various values of qm_R. Since at constant values of qm_R the curves are linear, the following equation may be written:

$$m_R = f(qm_R)m_f \tag{15}$$

The parameter $f(qm_R) = \frac{1 - \frac{qm_R}{81.65} \frac{\partial C_{N_T}/m_R}{\partial n}}{\frac{m_{add}}{m_R}}$ is given in figure 12 and, in the range of qm_R from 0 to 50 $\frac{lb}{ft^2} \frac{1}{deg}$, it may be fitted by the quadratic equation

$$f(qm_R) = 1 + 0.009082qm_R - 0.00004479q^2m_R^2 \tag{16}$$

Thus

$$m_R = \left(1 + 0.009082qm_R - 0.00004479q^2m_R^2\right)m_f \tag{17}$$

Equation (17) may be solved as a quadratic equation for m_R or, as was done in the present case, m_R may be determined by iteration.

The rigid wing-body lift-curve slopes calculated for the 68 flight test conditions by using equation (17) are listed in table IV along with identifying flight and run numbers and Mach numbers. These slopes are plotted in figure 13 as a function of Mach number.

Variation of rigid lift-curve slope, m_R, with Mach number.- In order to aid in the determination of a curve giving the variation of m_R with Mach number, the data were divided into the groups (1 to 14) shown in table IV. The weighted mean values of m_R at constant Mach number were calculated from the equation

$$m_{R_w} = \frac{\Sigma w m_R}{\Sigma w} \tag{18}$$

The weighting factor w for each m_R was calculated from standard formulas for determining weights with precision of measurement and data range considered (ref. 6, for example).

The weighted mean values of m_R listed in table IV are shown plotted at the group Mach number in figure 14(a). In order to establish a function or functions of Mach number by which all 68 points might be fitted simultaneously, the data shown in figure 14(a) were reduced to equivalent zero Mach number values by dividing the lift-curve slopes by the associated swept-wing Glauert factor as

$$m_{R_{M=0}} = m_R\sqrt{1 - M^2\cos^2\Lambda} \tag{19}$$

The results of this operation are shown in figure 14(b) in which it appears that the lift-curve slope follows a Glauert type variation up to a Mach number of about 0.70 above which it could be represented as varying linearly with $\frac{M}{\sqrt{1 - M^2\cos^2\Lambda}}$.

Each point in figure 14(b) represents a weighted observation for a limited Mach number range. In order to analyze the weighted observations over the complete Mach number range for comparison with the wind-tunnel data, the lift-curve slope data were used in two parts. Part I contained the data from groups 1 through 8 and was fitted by a standard weighted least-squares equation as

$$m_R = \frac{\Sigma w m_R \dfrac{1}{\sqrt{1 - M^2\cos^2\Lambda}}}{\Sigma w\left(\dfrac{1}{\sqrt{1 - M^2\cos^2\Lambda}}\right)^2} \tag{20}$$

From the data of table IV and equation (20), the variation of m_R with Mach number below 0.70 was found to be

$$m_R = \frac{0.08520}{\sqrt{1 - M^2\cos^2\Lambda}} \qquad (\text{for } M < 0.70) \tag{21}$$

with a standard error of fit of ± 0.0031. Part II contained the data from groups 7 through 14 and was fitted by an equation of the form

$$AwM + Bw = w\left(m_R - \frac{0.08520}{\sqrt{1 - M^2\cos^2\Lambda}}\right)\sqrt{1 - M^2\cos^2\Lambda} \qquad (22)$$

which in matrix form for solution of the coefficients A and B becomes

$$\begin{Bmatrix} A \\ B \end{Bmatrix} = \begin{bmatrix} \Sigma wM^2 & \Sigma wM \\ \Sigma wM^2 & \Sigma w \end{bmatrix}^{-1} \begin{Bmatrix} \Sigma wM\left(m_R - \frac{0.08520}{\sqrt{1 - M^2\cos^2\Lambda}}\right)\sqrt{1 - M^2\cos^2\Lambda} \\ \Sigma w\left(m_R - \frac{0.08520}{\sqrt{1 - M^2\cos^2\Lambda}}\right)\sqrt{1 - M^2\cos^2\Lambda} \end{Bmatrix} \qquad (23)$$

Solution of equation (23) for A and B gives the variation of m_R for Mach numbers above 0.68 as

$$m_R = \frac{0.03043 + 0.07974M}{\sqrt{1 - M^2\cos^2\Lambda}} \quad (\text{for } M > 0.68) \qquad (24)$$

with a standard error of ± 0.0031.

Comparison of flight and wind-tunnel rigid wing-body lift-curve slopes.- The variation of rigid lift-curve slope m_R with Mach number established by equations (21) and (24) from the basic data shown in figure 13 are plotted in figure 15 as the dashed lines. The solid-line curve shown in figure 15 is the variation of wind-tunnel rigid-model lift-curve slope (ref. 4 or 7) with Mach number. The agreement between flight and wind-tunnel values to a Mach number of 0.70 is seen to be excellent. This agreement indicates that standard theoretical procedures used to calculate flexible lift-curve slopes for flight conditions are entirely adequate for the Mach number range tested since the procedure used to obtain flexible values from rigid values is just the reverse of the procedure used in the present case. The disagreement above $M = 0.70$ may be viewed in several ways. From the standpoint of wind-tunnel testing techniques, it might be pointed out that the extrapolated flight test data depend on an assumed distribution of two-dimensional lift-curve slope across the span which may not have the same distribution at all Mach numbers. Also the estimated correction factor for total upwash effects gives a value of angle of attack

$$\alpha_2 \approx 0.91\alpha_1$$

which may be more in error at high Mach numbers than at low Mach numbers.

From a flight-testing-technique viewpoint, questions may be directed toward the validity of small-scale model tests at Mach numbers where tunnel disturbances may affect the results, or to the accuracy with which the model results were corrected for flexibility effects. Another possible source of difference between wind-tunnel test values and flight-test values lies in the fact that no blocking corrections were applied to the test-section Mach number. In reference 7 it was stated that the uncorrected test-section Mach numbers were believed to be accurate to within 2 percent up to $M = 0.85$. All in all, it is impossible to state which data best represent the rigid wing-body lift-curve slopes above $M = 0.70$.

Calculation of flexible wing-body lift-curve slopes.- When equations (21) and (24) are inserted in equation (17) for m_R, the flexible wing-body faired lift-curve slope m_F may be calculated for the flight test conditions. The calculated curves of m_F against M for altitudes of 20,000, 25,000, 30,000, and 35,000 feet for an average gross weight of 116,000 pounds are shown in figure 16. Also shown in figure 16 are the measured m_f values from figure 8. The family of curves is seen to fit the data of the four altitudes with a relatively small amount of scatter. Extrapolation of the data to lower altitudes is limited to a value of qm_R of $50 \frac{lb}{ft^2} \frac{1}{deg}$, the limit of the theoretical calculations made for this analysis. The calculations as noted previously correspond only to the wing stiffness distribution for airplanes of the type used in the present investigation and not to later versions of the same general configuration.

Angle-of-Zero-Lift Data

Direct measurements of the angles of zero lift were not available from the flight test data since the airplane was restricted to flight at positive load factors. Thus a comparison of wind-tunnel and flight data was necessarily based on extrapolated values of angle of attack obtained from least-squares solutions. These extrapolated values of angle of zero lift α_o are listed in table V. The extrapolation by least-squares analysis gives an intercept or α_o value which could also be expressed by the following equation:

$$\alpha_o = \overline{\alpha_3} - \frac{1}{a_m} \overline{C_{N_{A_C}}} \tag{25a}$$

Inasmuch as the faired values of lift-curve slope m_F in figure 16 corrected for tail-on conditions more nearly represent the true lift-curve slope than the individual lift-curve slope m_f with its inevitable scatter, the angle of zero lift associated with the faired lift-curve slope

was desired in order to represent best the data of $C_{N_{A_C}}$ plotted against α_3 in the range of the measurements. The corrected angle of zero lift would be given by the equation

$$\alpha_{o_C} = \overline{\alpha_3} - \frac{1}{a_F} \overline{C_{N_{A_C}}} \tag{25b}$$

From equations (25a) and (25b), the corrected angle of zero lift consistent with a faired lift-curve slope and representing the data in the range of the measurements becomes

$$\alpha_{o_C} = \alpha_o - \overline{C_{N_{A_C}}}\left(\frac{1}{a_F} - \frac{1}{a_m}\right) \tag{26}$$

This procedure was used to calculate corrected values α_{o_C} for each of the 68 runs, the results being shown in table V and plotted in figure 17 as a function of Mach number. It is evident from figure 17 that an analysis of the data in this form is next to impossible. Although in a given flight there appears to be a trend with Mach number, the scatter of the data from flight to flight suggests the presence of zero shifts in the recorded angles of attack. These suspected zero shifts in no way affect the magnitude or validity of the correction applied through equation (26).

Calculation of $\alpha_{o_{WB}}$.- For trimmed level flight, the following expression for airplane normal-force coefficient may be written

$$C_{N_{A_{trim}}} = m_F\left(\alpha_{trim} - \alpha_{o_{WB}}\right) + \left(\frac{\partial C_N}{\partial \alpha}\right)_{tail}\left(1 - \frac{d\epsilon}{d\alpha}\right)\frac{S_t}{S}\alpha_{trim} -$$

$$2.75\,\frac{d\epsilon}{d\alpha}\left(\frac{\partial C_N}{\partial \alpha}\right)_{tail}\frac{S_t}{S} + \left(\frac{\partial C_N}{\partial \delta}\right)_{tail}\frac{S_t}{S}\delta_{trim} \tag{27a}$$

or

$$C_{N_{A_{trim}}} = m_F\left(\alpha_{trim} - \alpha_{o_{WB}}\right) + K_1\,\alpha_{trim} - 2.75K_2 + K_3\,\delta_{trim} \tag{27b}$$

From equation (27b) and the equation

$$\alpha_{trim} = \alpha_{o_C} + \frac{C_{N_{A_{trim}}}}{a_F} \tag{28}$$

an expression for $\alpha_{o_{WB}}$ may be derived as follows:

$$\alpha_{o_{WB}} = \alpha_{o_C} + \frac{1}{m_F}\left(K_1 \alpha_{o_C} - 2.75K_2 + K_3 \delta_{trim}\right) + C_{N_{A_{trim}}}\left(-\frac{1}{m_F} + \frac{K_1}{m_F a_F} + \frac{1}{a_F}\right) \tag{29}$$

Values of $\alpha_{o_{WB}}$ were calculated from equation (29) by using preliminary values of K_1, K_2, and K_3 based on an unpublished analysis of the tail loads with angle of attack by the authors of the present paper and values of α_{o_C}, m_F, and a_F already determined in the present paper as well as the measured trim root elevator angles δ_{trim} and normal-force coefficients $C_{N_{A_{trim}}}$. The results are tabulated in table V and plotted in figure 18. Although considerable scatter still exists in the data from flight to flight, the data in any given flight show no consistent variation with Mach number. Dynamic pressure or flexibility effects are not evident either since data for flight 12, which consist of maneuvers at three different altitudes, exhibit no separation with altitude.

Weighted mean values of $\alpha_{o_{WB}}$ are also listed in table V for each flight. The differences exhibited between weighted values of $\alpha_{o_{WB}}$ from flight to flight may be due to unavoidable errors in ground-zeroing procedures. A weighted mean value of $\alpha_{o_{WB}}$ was determined from all 68 maneuvers as

$$\overline{\alpha_{o_{WB}}} = -3.13^\circ$$

Design data (ref. 4) based on wind-tunnel data listed the angle of zero lift of the wing-fuselage configuration as -0.5° with respect to the wing root chord line or -3.25° with respect to the present reference, the fuselage axis. In addition, it was stated in reference 4 that there was no discernible variation with Mach number. The agreement between flight and wind-tunnel values of $\alpha_{o_{WB}}$ is considered to be excellent.

Calculation of tail on α_o.- With a mean value of $\alpha_{o_{WB}}$ established as constant for all flights and runs, an adjusted value of α_o for tail-on flight conditions may be calculated as

$$\alpha_{o_{adj}} = -3.13 - \alpha_{o_{WB}} + \alpha_{o_C} \tag{30}$$

The results of these computations are listed in table V and plotted in figure 19. The differences exhibited in figure 19 are a result of variations of tail-on lift-curve slope, downwash, and elevator effectiveness with Mach number as well as fuselage flexibility effects but these differences are not sufficiently great to warrant further analysis.

DISCUSSION

Analysis of the test results indicates that numerous corrections must be made to the measured data if proper values of lift-curve slopes are to be obtained from the type of nose-boom angle-of-attack installation used. The size of the corrections may be reduced but not eliminated by lengthening the boom (reducing interference effects) and stiffening the boom (reducing inertia effects). The particular corrections required to account for lag in the present case may, of course, be eliminated by the use of a better recording instrument. Corrections for angular velocity effects may be reduced somewhat if a slow windup turn type of maneuver is used. The windup turn maneuver is not necessarily a more suitable maneuver since speed changes and roll and sideslip effects would then have to be considered in an analysis of the data. Another undesirable feature of the windup turn maneuver is the reduced range of angles of attack available for which normal-force coefficients are linear with angle of attack.

The importance of obtaining a large amount of data with duplication of maneuvers at similar flight conditions is a factor which is sometimes overlooked. In the most carefully conducted flight test program with carefully corrected measurements, considerable scatter may still exist in the results. Least-squares procedures may be used to analyze results where scatter is present only if sufficient data are available with a reasonable range of variables. A good fit to the data is not proof that the coefficients derived in the process are final correct answers.

The determination of equivalent rigid values of lift-curve slope from flight measurements on a flexible airplane requires a careful analysis of the data. As pointed out previously, a certain amount of scatter is unavoidable; thus, simplified plotting techniques, even if the correct flexibility parameters are chosen, seldom produce curves that may be extrapolated to rigid conditions. In view of the fact that the basic flexibility parameter qm_R is the product of the dynamic pressure q and the unknown rigid lift-curve slope m_R, the use of a plotting technique is doubly difficult. It is thus necessary to reduce the flight data to equivalent rigid values by theoretical load distribution calculations and calculated or experimental deflection characteristics. Since the basis of the theoretical load distribution calculations is an adequate

determination of the two-dimensional wing lift-curve slope distribution, the whole process is unfortunately somewhat dependent on wind-tunnel pressure-distribution tests. When the reverse process is used, that is, the calculation of flight test values from wind-tunnel tests and theory, the same accurate basic information is required.

CONCLUDING REMARKS

Flight measurements of airplane lift-curve slopes and angles of zero lift for a large flexible swept-wing airplane as obtained for 68 push-pull maneuvers in a Mach number range from 0.42 to 0.81 at altitudes from 20,000 to 35,000 feet have been presented.

The lift-curve slopes obtained from flight conditions where flexibility is a factor were analyzed to determine airplane tail-off rigid-wing values which showed excellent agreement with rigid wind-tunnel data for a model of the airplane up to a Mach number of 0.70. In the Mach number range from 0.70 to 0.81, however, the flight rigid values of lift-curve slope show a more rapid increase with Mach number than the wind-tunnel data.

The agreement obtained between flight and wind-tunnel results indicates that in the Mach number range tested standard design calculation methods would accurately predict flexible lift-curve slopes if the basic two-dimensional lift-curve-slope data and wing-stiffness data are accurate.

Analysis of angles of zero lift for tail-off conditions indicated good agreement with wind-tunnel results both in magnitude and in lack of variation with Mach number.

In the course of the investigation and as detailed in the present paper, new approaches to analysis procedures believed to be of interest were used. Specifically these were (a) the determination during abrupt maneuvers of lift-curve slopes from instrumentation which had a large amount of lag and (b) the conversion of flight measurements of lift-curve slopes on a flexible airplane to rigid conditions according to physically correct equations.

Langley Aeronautical Laboratory,
National Advisory Committee for Aeronautics,
Langley Field, Va., May 9, 1956.

APPENDIX

CORRECTIONS TO BASIC DATA

Corrections to Angle-of-Attack Measurements

At any instant in a maneuver, the measured angle of attack at the vane (assuming no alinement errors and that the floating angle is zero) is related to the true angle of attack of the airplane through the following equation:

$$\alpha_1 = \alpha_2 + \left(\mu_{wing} + \mu_{boom} + \mu_{fuselage} + \Delta\alpha_{l_{\dot{\theta}}} + \Delta\alpha_{l_i} + \Delta\alpha_{l_a}\right) \qquad (A1)$$

where the terms in parenthesis are in the nature of small corrections due to upwash, pitching velocity, and boom bending.

The upwash at the vane due to the wing may be calculated from the following expression which uses a swept-horseshoe-vortex system to determine the flow direction at points in space not on the quarter-chord line of the wing:

$$\mu_{wing} = -\frac{c l_\alpha}{2\pi AR}\left[1 - \frac{\sqrt{(\tau + \tan\Lambda)^2 + 1} - \frac{\tau \tan\Lambda}{|\tau|}}{\tau}\right](\alpha_W) \qquad (A2)$$

The angle of attack of the wing is the angle of attack of the fuselage reference axis plus the wing incidence angle of 2.75°. With numerical values inserted, equation (A2) becomes

$$\mu_{wing} = 0.0446(\alpha_2 + 2.75)$$

(Since this is a correction, an average value of $c l_\alpha = 0.100$ was used.)

The upwash at the vane due to the flow around the boom may be estimated with good accuracy from the equation for two-dimensional flow around a cylinder as

$$\mu_{boom} = \left(\frac{r}{y}\right)^2 \alpha_2 \qquad (A3)$$

With numerical values inserted, this becomes

$$\mu_{boom} = 0.0135\alpha_2$$

The upwash induced at the vane from the fuselage based on some very limited flight test data is approximated by

$$\mu_{fuselage} = \left(\frac{r}{x}\right)^2 \alpha_2 \tag{A4}$$

Substituting the dimensions of the fuselage radius at the original nose, equation (A4) is numerically equal to

$$\mu_{fuselage} = 0.0375\alpha_2$$

Equation (A1) may be rewritten as

$$\alpha_2 = \frac{\alpha_1 - 0.12 - \Delta\alpha_{l_{\dot{\theta}}} - \Delta\alpha_{l_i} - \Delta\alpha_{l_a}}{1 + 0.0446 + 0.0135 + 0.0375} \tag{A5}$$

or

$$\alpha_2 = 0.913\left(\alpha_1 - 0.12 - \Delta\alpha_{l_{\dot{\theta}}} - \Delta\alpha_{l_i} - \Delta\alpha_{l_a}\right)$$

The correction due to the aerodynamic loading $\Delta\alpha_{l_a}$ on the boom was found to be so small that even at the highest dynamic pressure of the tests the measuring error due to this parameter would be less than 0.01°.

The pitching-velocity correction term is

$$\Delta\alpha_{l_{\dot{\theta}}} = \frac{-x_v\dot{\theta}}{V}$$

With x_v equal to 58 feet and V measured in feet per second, $\dot{\theta}$ in radians per second, and $\Delta\alpha_{l_{\dot{\theta}}}$ in degrees, the pitching-velocity correction term becomes

$$\Delta\alpha_{l_{\dot{\theta}}} = -3323\,\frac{\dot{\theta}}{V} \tag{A6}$$

The negative sign is due to the fact that positive pitching velocities deflect the vane tail downward relative to the boom (a negative indication of angle of attack).

The boom inertia bending correction term $\Delta\alpha_{l_i}$ was calculated by using measured influence coefficients and the known weight distribution of the boom and head as

$$\Delta\alpha_{l_i} = -0.353\left(n_{boom} - 1\right)$$

The negative sign results from positive load factors decreasing the angle between the boom and the vane axis.

With

$$n_{boom} = n_m + \frac{\ddot{\theta}}{g}(\text{distance between vane axis and accelerometer})$$

then

$$\Delta\alpha_{l_i} = -0.353\left(n_m - 1\right) - 0.650\ddot{\theta} \tag{A7}$$

The substitution of equations (A6) and (A7) into equation (A5) with $\Delta\alpha_{l_a} = 0$ results in the equation used to correct the flight measurements of angle of attack:

$$\alpha_2 = 0.91\alpha_1 - 0.11 + 3034\,\frac{\dot{\theta}}{V} + 0.322\left(n_m - 1\right) + 0.593\ddot{\theta} \tag{A8}$$

Corrections to Airplane Normal-Force Coefficients

The airplane normal-force coefficient is defined as

$$C_{N_A} = \frac{n_{cg}W}{qS} \tag{A9}$$

Since normal-load factors were measured with NACA accelerometers mounted at fuselage station 638 (34.2 percent of the wing M.A.C.), a correction is required to the measured load factor to determine the normal-force coefficient for particular center-of-gravity positions. Thus, equation (A9) becomes

$$C_{N_A} = \frac{n_m W}{qS} + \frac{d}{g}\,\frac{W}{qS}\,\ddot{\theta} \tag{A10}$$

where d is the distance between the accelerometer and the center of gravity.

With numerical values inserted, equation (A10) becomes

$$C_{N_A} = \frac{n_m W}{qS} + \frac{0.402W}{qS}\left(0.342 - \frac{\text{c.g.}}{100}\right)\ddot{\theta} \tag{A11}$$

During the maneuvers used for the analysis of the data of the present report, pitching accelerations as high as ±0.5 radians/sec^2 were encountered. Since the airplane is out of trim whenever appreciable pitching accelerations exist, the angle of attack and the airplane normal-force coefficients are no longer linearly related. A correction can be made to the values of C_{N_A}, deduced from the data by assuming that $\Delta C_{N_{\ddot{\theta}}}$ (the vertical-reaction load coefficient due to pitch) is proportional to the pitching moment of inertia tail load as follows:

$$\Delta C_{N_{\ddot{\theta}}} = \frac{dL_T}{d\ddot{\theta}} \frac{\ddot{\theta}}{qS} \tag{A12}$$

An estimated average value of 28,000 lb/radian/sec^2 based on an average pitching moment of inertia was used for $dL_T/d\ddot{\theta}$. The value of airplane normal-force coefficient for trimmed flight corresponding to the corrected angle of attack α_2 becomes

$$C_{N_{A_C}} = \frac{n_m W}{qS} + \frac{0.402W}{qS}\left(0.342 - \frac{c.g.}{100}\right)\ddot{\theta} + \frac{19.61}{q}\ddot{\theta} \tag{A13}$$

REFERENCES

1. Donegan, James J., and Huss, Carl R.: Study of Some Effects of Structural Flexibility on the Longitudinal Motions and Loads as Obtained From Flight Measurements of a Swept-Wing Bomber. NACA RM L54L16, 1954.

2. Brown, R. B., Holtby, K. F., and Martin, H. C.: A Superposition Method for Calculating the Aeroelastic Behavior of Swept Wings. Jour. Aero. Sci., vol. 18, no. 8, Aug. 1951, pp. 531-542.

3. Gray, W. L., and Schenk, K. M.: A Method for Calculating the Subsonic Steady-State Loading on an Airplane With a Wing of Arbitrary Plan Form and Stiffness. NACA TN 3030, 1953.

4. Gray, E. Z., Sandoz, P., and Entz, H.: Design Load Criteria. [Model 13-47B.] Vol. I. Document no. D-9441 (Contract No. W33-038 ac-22413), Boeing Airplane Co., Nov. 9, 1948.

5. Mayo, Alton P., and Ward, John F.: Experimental Influence Coefficients for the Deflection of the Wing of a Full-Scale, Swept-Wing Bomber. NACA RM L53L23, 1954.

6. Merriman, Mansfield: Method of Least Squares. Eighth ed., John Wiley & Sons, Inc., 1911.

7. Budish, Nathan N.: Longitudinal Stability at High Airspeeds. [Model XB-47.] Document No. D-8603-0 (Contract No. W33-038 ac-22413), Boeing Airplane Co., Feb. 29, 1952.

TABLE I.- TEST AIRPLANE CHARACTERISTICS AND DIMENSIONS

Total wing area, sq ft	1,428
Wing span, ft	116
Wing aspect ratio	9.42
Wing taper ratio	0.42
Wing mean aerodynamic chord, ft	13
Wing sweepback (25-percent-chord line), deg	35
Total horizontal-tail area, sq ft	268
Airfoil section	BAC 145
Airfoil thickness ratio (parallel to center line), percent	12

TABLE II.- SUMMARY OF FLIGHT CONDITIONS

Flight	Run	M_{av}	q_{av}, lb/sq ft	Pressure altitude, ft	W, lb	Center-of-gravity location, percent M.A.C.
2	27	0.636 ± 0.002	137 ± 2	35,200	112,600	21.1
	28	0.735 ± 0.001	184 ± 1	34,900	112,300	21.3
	29	0.796 ± 0.004	216 ± 2	34,800	112,200	21.5
3	11	0.750 ± 0.001	196 ± 1	34,600	120,300	13.6
	12	0.728 ± 0.007	188 ± 5	34,100	120,100	13.6
	13	0.689 ± 0.006	167 ± 3	34,400	119,900	13.5
	14	0.631 ± 0.002	140 ± 1	34,600	119,000	13.4
4	19	0.699 ± 0.002	264 ± 3	25,000	108,900	21.0
	20	0.591 ± 0.001	190 ± 1	25,000	108,700	20.9
	21	0.486 ± 0.003	128 ± 1	25,300	108,400	20.8
6	11	0.789 ± 0.001	264 ± 3	30,800	108,800	13.1
	12	0.790 ± 0.001	268 ± 1	30,500	108,700	13.1
	13	0.741 ± 0.001	244 ± 1	29,800	108,400	13.1
	14	0.690 ± 0.001	215 ± 1	29,400	108,200	13.2
	15	0.643 ± 0.003	187 ± 2	29,400	107,600	13.0
8	4	0.544 ± 0.008	163 ± 4	24,900	124,800	22.6
	5	0.648 ± 0.004	233 ± 3	24,800	124,500	22.8
	6	0.758 ± 0.002	314 ± 4	25,100	124,000	23.2
9	1	0.598 ± 0.003	125 ± 1	34,800	126,700	22.6
	2	0.647 ± 0.004	147 ± 2	34,900	126,200	22.5
	3	0.681 ± 0.001	161 ± 1	35,200	126,100	22.7
	4	0.731 ± 0.003	185 ± 1	35,200	125,700	22.9
	5	0.779 ± 0.002	214 ± 1	34,900	125,400	23.1
	6	0.795 ± 0.001	216 ± 1	35,500	125,200	23.3
	7	0.810 ± 0	225 ± 1	35,300	124,900	23.5
10	3	0.598 ± 0.003	159 ± 2	29,800	127,200	22.6
	4	0.647 ± 0.001	185 ± 0	29,900	126,500	22.3
	5	0.681 ± 0.001	200 ± 1	30,500	126,300	22.4
	6	0.726 ± 0.001	230 ± 1	30,200	126,100	22.5
	7	0.763 ± 0	254 ± 0	30,200	125,400	23.0
	8	0.789 ± 0.001	260 ± 1	31,100	125,200	23.1
	9	0.812 ± 0.001	274 ± 1	31,300	124,900	23.3
11	11	0.495 ± 0.003	138 ± 1	24,400	109,200	21.8
	12	0.542 ± 0.003	164 ± 1	24,600	108,900	21.7
	13	0.597 ± 0.001	194 ± 1	25,100	108,500	21.8
	14	0.636 ± 0	222 ± 0	25,000	108,500	21.8
	15	0.681 ± 0	247 ± 0	25,700	108,400	21.9
	16	0.702 ± 0.001	266 ± 1	25,400	107,800	21.7
	17	0.734 ± 0	291 ± 0	25,300	107,500	21.8
	24	0.427 ± 0.001	126 ± 1	19,700	103,700	22.2
12	6	0.584 ± 0.001	127 ± 1	33,700	120,400	14.5
	7	0.642 ± 0.001	147 ± 1	34,400	120,300	14.6
	8	0.679 ± 0.001	162 ± 0	34,900	119,900	14.6
	9	0.721 ± 0.001	178 ± 1	35,300	119,600	14.6
	10	0.773 ± 0.001	202 ± 1	35,400	119,100	14.7
	11	0.790 ± 0	215 ± 0	35,200	118,800	14.6
	12	0.812 ± 0	228 ± 0	35,200	118,700	14.4
	17	0.483 ± 0.001	130 ± 1	24,600	116,600	13.8
	18	0.532 ± 0	157 ± 0	24,700	116,500	13.7
	19	0.600 ± 0.001	198 ± 1	24,900	116,400	13.7
	20	0.637 ± 0	223 ± 0	25,000	116,300	13.8
	21	0.682 ± 0.001	255 ± 1	25,000	116,100	13.9
	22	0.694 ± 0.001	262 ± 0	25,200	115,800	14.1
	23	0.735 ± 0.001	298 ± 1	24,900	115,400	14.3
	24	0.642 ± 0.002	279 ± 3	20,000	111,100	21.5
	25	0.595 ± 0.002	242 ± 1	19,800	111,100	21.5
	26	0.543 ± 0	202 ± 1	19,700	110,600	21.6
	27	0.482 ± 0.002	159 ± 1	19,700	110,300	21.9
	28	0.427 ± 0.001	126 ± 1	19,600	110,200	21.6
16	1	0.642 ± 0.001	282 ± 1	19,900	117,100	14.6
	2	0.599 ± 0.002	246 ± 2	19,800	116,800	14.3
	3	0.542 ± 0.002	200 ± 2	20,000	116,600	13.6
	4	0.482 ± 0.002	160 ± 1	19,800	116,000	13.9
	5	0.428 ± 0.003	127 ± 2	19,500	115,500	13.7
	6	0.433 ± 0.002	131 ± 2	19,300	115,100	13.5
17	5	0.808 ± 0.001	364 ± 1	24,600	116,400	14.2
	6	0.762 ± 0	326 ± 0	24,500	116,200	14.2
	7	0.725 ± 0	295 ± 0	24,500	115,600	14.0

TABLE III.- VALUES OF LIFT-CURVE SLOPE AND ANGLE OF ZERO LIFT

DETERMINED FROM ANALYSIS OF INDIVIDUAL RUNS

Pressure altitude, ft	Flight	Run	M_{av}	q_{av}, lb/sq ft	a_m, per deg	α_o, deg	Number of points used	Standard error, s, deg
20,000	11	24	0.427	126	0.0815	-3.17	23	±0.07
	12	28	.427	126	.0878	-2.78	32	±.10
	16	5	.428	127	.0848	-2.55	25	±.08
	16	6	.433	131	.0846	-2.53	37	±.07
	12	27	.482	159	.0884	-2.71	39	±.12
	16	4	.482	160	.0855	-2.54	33	±.08
	16	3	.542	200	.0845	-2.65	32	±.08
	12	26	.543	202	.0847	-2.79	37	±.09
	12	25	.595	242	.0829	-2.82	36	±.09
	16	2	.599	246	.0843	-2.71	34	±.10
	12	24	.642	279	.0795	-3.01	35	±.11
	16	1	.642	282	.0824	-2.83	34	±.07
25,000	12	17	0.483	130	0.0847	-2.96	23	±0.11
	4	21	.486	128	.0838	-3.35	20	±.08
	11	11	.495	138	.0854	-3.04	26	±.11
	12	18	.532	157	.0850	-2.88	24	±.08
	11	12	.542	164	.0857	-3.03	32	±.09
	8	4	.544	163	.0839	-3.21	27	±.05
	4	20	.591	190	.0894	-2.97	23	±.09
	11	13	.597	194	.0866	-2.98	32	±.06
	12	19	.600	198	.0815	-3.00	26	±.14
	11	14	.636	222	.0860	-3.03	28	±.06
	12	20	.637	223	.0835	-2.95	32	±.11
	8	5	.648	233	.0815	-3.28	36	±.09
	11	15	.681	247	.0882	-2.97	30	±.07
	12	21	.682	255	.0845	-2.98	22	±.08
	12	22	.694	262	.0863	-2.83	24	±.08
	4	19	.699	264	.0881	-3.17	26	±.06
	11	16	.702	266	.0877	-2.95	25	±.06
	17	7	.725	295	.0918	-2.69	20	±.07
	11	17	.734	291	.0903	-3.00	22	±.07
	12	23	.735	298	.0837	-2.94	26	±.08
	8	6	.758	314	.0907	-2.97	34	±.05
	17	6	.762	326	.0899	-2.72	26	±.09
	17	5	.808	364	.0956	-2.68	27	±.09
30,000	10	3	0.598	159	0.0904	-2.67	37	±0.09
	6	15	.643	187	.0857	-2.93	35	±.04
	10	4	.647	185	.0887	-2.79	48	±.11
	10	5	.681	200	.0964	-2.44	29	±.07
	6	14	.690	215	.0876	-2.87	21	±.04
	10	6	.726	230	.0921	-2.75	38	±.08
	6	13	.741	244	.0869	-3.00	29	±.05
	10	7	.763	254	.1001	-2.57	25	±.04
	6	11	.789	264	.0954	-2.84	40	±.06
	6	12	.790	268	.1009	-2.61	21	±.06
	10	8	.789	260	.1001	-2.71	23	±.06
	10	9	.812	274	.1033	-2.69	34	±.07
35,000	12	6	0.584	127	0.0849	-3.00	28	±0.10
	9	1	.598	125	.0896	-2.71	30	±.12
	3	14	.631	140	.0830	-3.45	28	±.04
	2	27	.636	137	.0932	-2.74	31	±.03
	12	7	.642	147	.0883	-2.82	25	±.10
	9	2	.647	147	.0935	-2.59	41	±.12
	12	8	.679	162	.0887	-2.86	23	±.15
	9	3	.681	161	.0941	-2.67	37	±.10
	3	13	.689	167	.0853	-3.51	28	±.07
	12	9	.721	178	.0928	-2.87	24	±.13
	3	12	.728	188	.0922	-3.22	36	±.04
	9	4	.731	185	.1006	-2.42	29	±.08
	2	28	.735	184	.1018	-2.59	29	±.04
	3	11	.750	196	.0953	-3.10	26	±.05
	12	10	.773	202	.0973	-2.86	19	±.08
	9	5	.779	214	.1032	-2.48	44	±.11
	12	11	.790	215	.1015	-2.72	22	±.11
	9	6	.795	216	.1056	-2.54	34	±.12
	2	29	.796	216	.1134	-2.30	25	±.03
	9	7	.810	225	.1073	-2.64	33	±.10
	12	12	.812	228	.1055	-2.67	21	±.09

TABLE IV.- RIGID WING-BODY VALUES OF LIFT-CURVE SLOPE

Group	Flight	Run	Run Mach number	Group Mach number	Weighting factor, w	m_R (eq. (17))	m_{R_w} (eq. (18))
1	11	24	0.427	0.429	21	0.0870	0.0931
	12	28	.427		19	.0953	
	16	5	.428		15	.0950	
	16	6	.433		29	.0950	
2	12	27	0.482	0.486	17	0.0984	0.0946
	16	4	.482		10	.0978	
	12	17	.483		20	.0925	
	4	21	.486		13	.0919	
	11	11	.495		23	.0936	
3	12	18	0.532	0.541	16	0.0955	0.0960
	11	12	.542		28	.0960	
	16	3	.542		9	.0996	
	12	26	.543		16	.0969	
	8	4	.544		16	.0936	
4	12	6	0.584	0.595	39	0.0933	0.0968
	4	20	.591		9	.1029	
	12	25	.595		15	.0966	
	11	13	.597		18	.0990	
	10	3	.598		22	.1008	
	9	1	.598		36	.0971	
	16	2	.599		9	.1010	
	12	19	.600		25	.0930	
5	3	14	0.631	0.635	14	0.0935	0.0983
	2	27	.636		10	.1036	
	11	14	.636		17	.1003	
	12	20	.637		19	.0971	
6	12	7	0.642	0.644	34	0.0990	0.0991
	12	24	.642		13	.0941	
	16	1	.642		10	.1011	
	6	15	.643		6	.1002	
	9	2	.647		30	.1042	
	10	4	.647		27	.1003	
	8	5	.648		31	.0946	
7	12	8	0.679	0.681	37	0.0998	0.1034
	9	3	.681		35	.1051	
	10	5	.681		8	.1117	
	11	15	.681		16	.1050	
	12	21	.682		9	.1012	
8	3	13	0.689	0.695	17	0.0982	0.1029
	6	14	.690		4	.1047	
	12	22	.694		10	.1046	
	4	19	.699		7	.1062	
	11	16	.702		15	.1052	
9	12	9	0.721	0.726	16	0.1072	0.1103
	17	7	.725		4	.1151	
	10	6	.726		11	.1080	
	3	12	.728		15	.1085	
	9	4	.731		14	.1160	
10	11	17	0.734	0.736	7	0.1106	0.1081
	12	23	.735		13	.1031	
	2	28	.735		5	.1186	
	6	13	.741		2	.1055	
11	3	11	0.750	0.758	4	0.1135	0.1150
	8	6	.758		11	.1126	
	17	6	.762		10	.1147	
	10	7	.763		5	.1219	
12	12	10	0.773	0.776	17	0.1140	0.1185
	9	5	.779		20	.1224	
13	6	11	0.789	0.791	3	0.1200	0.1246
	10	8	.789		4	.1213	
	6	12	.790		2	.1280	
	12	11	.790		11	.1225	
	9	6	.795		15	.1257	
	2	29	.796		2	.1386	
14	17	5	0.808	0.810	5	0.1262	0.1285
	9	7	.810		11	.1290	
	10	9	.812		5	.1280	
	12	12	.812		6	.1297	

TABLE V.- ANGLE-OF-ZERO-LIFT DETERMINATION

Flight	Run	M	α_o, deg	α_{o_C} (eq. (26)), deg	$\alpha_{o_{WB}}$ (eq. (29)), deg	$\alpha_{o_{WB}}$ (weighted mean), deg	$\alpha_{o_{adj}}$ (eq. (30)), deg
2	27	0.636	-2.74	-2.94	-3.16	-3.06	-2.91
	28	.735	-2.59	-2.83	-3.11		-2.85
	29	.796	-2.30	-2.60	-2.92		-2.81
3	11	0.750	-3.10	-3.08	-3.40	-3.47	-2.81
	12	.728	-3.22	-3.16	-3.49		-2.80
	13	.689	-3.51	-3.26	-3.54		-2.85
	14	.631	-3.45	-3.17	-3.43		-2.87
4	19	0.699	-3.17	-3.21	-3.51	-3.49	-2.83
	20	.591	-2.97	-3.19	-3.43		-2.91
	21	.486	-3.35	-3.31	-3.52		-2.92
6	11	0.789	-2.84	-2.81	-3.14	-3.11	-2.80
	12	.790	-2.61	-2.73	-3.07		-2.79
	13	.741	-3.00	-2.80	-3.07		-2.86
	14	.690	-2.87	-2.89	-3.14		-2.88
	15	.643	-2.93	-2.92	-3.15		-2.90
8	4	0.544	-3.21	-3.14	-3.38	-3.27	-2.89
	5	.648	-3.28	-3.04	-3.26		-2.91
	6	.758	-2.97	-2.91	-3.22		-2.82
9	1	0.598	-2.71	-2.67	-2.96	-2.98	-2.84
	2	.647	-2.59	-2.79	-3.01		-2.91
	3	.681	-2.67	-2.78	-3.06		-2.85
	4	.731	-2.43	-2.61	-2.89		-2.85
	5	.779	-2.48	-2.54	-2.85		-2.82
	6	.795	-2.54	-2.60	-2.95		-2.78
	7	.810	-2.64	-2.69	-3.09		-2.73
10	3	0.598	-2.67	-2.83	-3.10	-3.05	-2.86
	4	.647	-2.79	-2.79	-3.04		-2.88
	5	.681	-2.44	-2.75	-3.01		-2.87
	6	.726	-2.75	-2.74	-3.03		-2.84
	7	.763	-2.57	-2.68	-2.97		-2.84
	8	.789	-2.71	-2.72	-3.07		-2.78
	9	.812	-2.69	-2.73	-3.12		-2.74
11	11	0.495	-3.04	-3.04	-3.26	-3.25	-2.91
	12	.542	-3.03	-3.07	-3.27		-2.93
	13	.597	-2.98	-3.03	-3.24		-2.92
	14	.636	-3.03	-3.05	-3.28		-2.90
	15	.681	-2.97	-3.04	-3.28		-2.89
	16	.702	-2.95	-2.95	-3.21		-2.87
	17	.734	-3.00	-3.00	-3.29		-2.84
	24	.427	-3.17	-2.80	-3.10		-2.83
12	6	0.584	-3.00	-2.72	-3.04	-3.12	-2.81
	7	.642	-2.82	-2.75	-3.05		-2.83
	8	.679	-2.86	-2.73	-3.06		-2.80
	9	.721	-2.87	-2.82	-3.13		-2.82
	10	.773	-2.86	-2.77	-3.15		-2.75
	11	.790	-2.72	-2.73	-3.10		-2.76
	12	0.812	-2.67	-2.72	-3.15		-2.70
	17	.483	-2.96	-2.93	-3.28		-2.78
	18	.532	-2.88	-2.92	-3.19		-2.86
	19	.600	-3.00	-2.77	-3.06		-2.84
	20	.637	-2.95	-2.86	-3.15		-2.84
	21	.682	-2.98	-2.94	-3.21		-2.86
	22	0.694	-2.83	-2.84	-3.12		-2.85
	23	.735	-2.94	-2.75	-3.04		-2.84
	24	.642	-3.01	-2.84	-3.09		-2.88
	25	.595	-2.82	-2.79	-3.01		-2.91
	26	.543	-2.79	-2.85	-3.07		-2.91
	27	.482	-2.71	-2.97	-3.20		-2.90
	28	.427	-2.78	-3.06	-3.32		-2.87
16	1	0.642	-2.83	-2.85	-3.08	-3.02	-2.90
	2	.599	-2.71	-2.82	-3.08		-2.87
	3	.542	-2.65	-2.83	-3.03		-2.93
	4	.482	-2.54	-2.81	-2.97		-2.97
	5	.428	-2.55	-2.83	-2.98		-2.98
	6	.433	-2.53	-2.79	-2.94		-2.98
17	5	0.808	-2.68	-2.67	-3.06	-3.05	-2.74
	6	.762	-2.72	-2.68	-3.01		-2.80
	7	.725	-2.69	-2.80	-3.09		-2.84

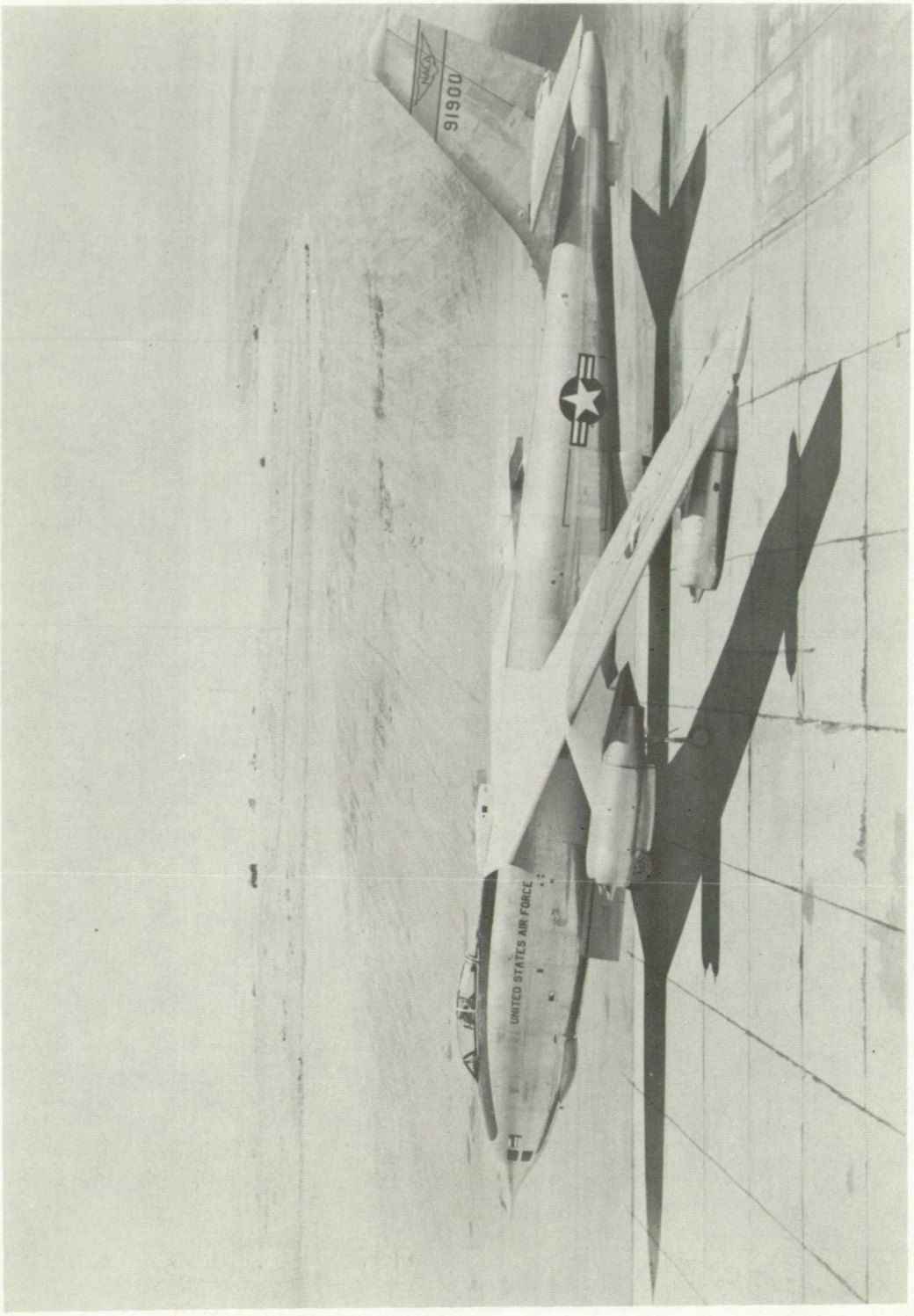

L-86692

Figure 1.- Side view of test airplane.

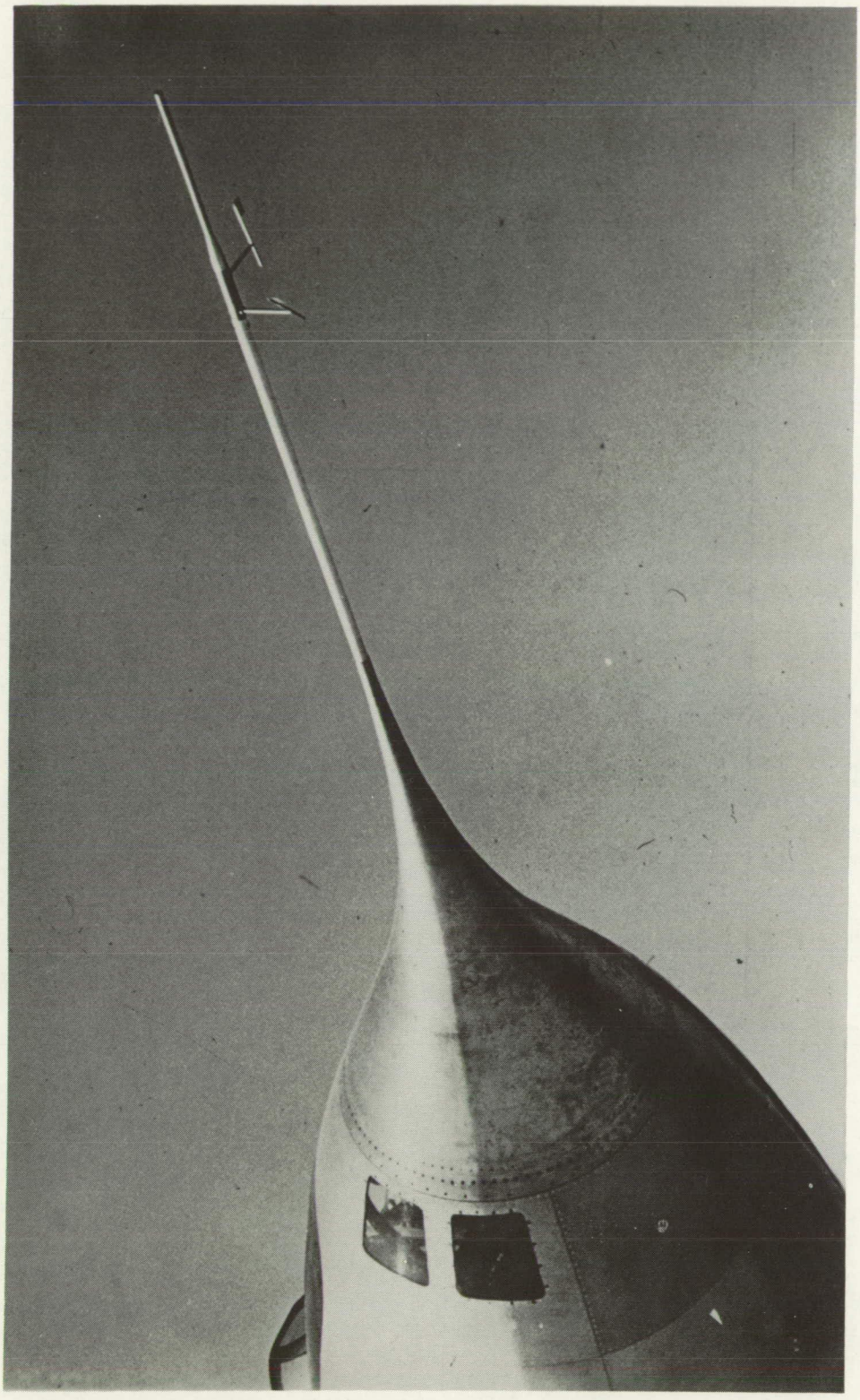

L-79626

Figure 2.- Nose-boom, angle-of-attack, and airspeed installations.

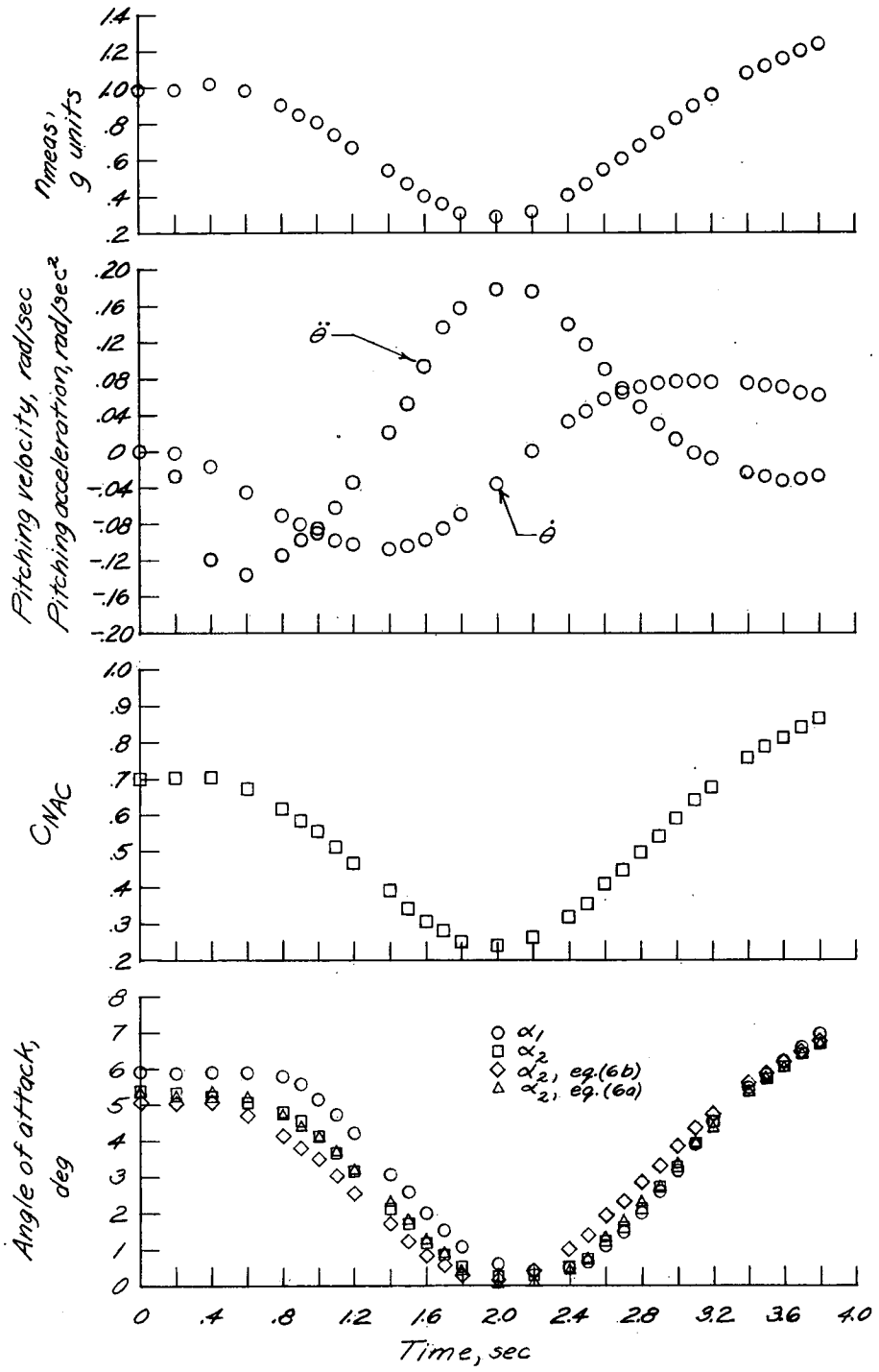

Figure 3.- Time histories of measured and calculated quantities for flight 9, run 1.

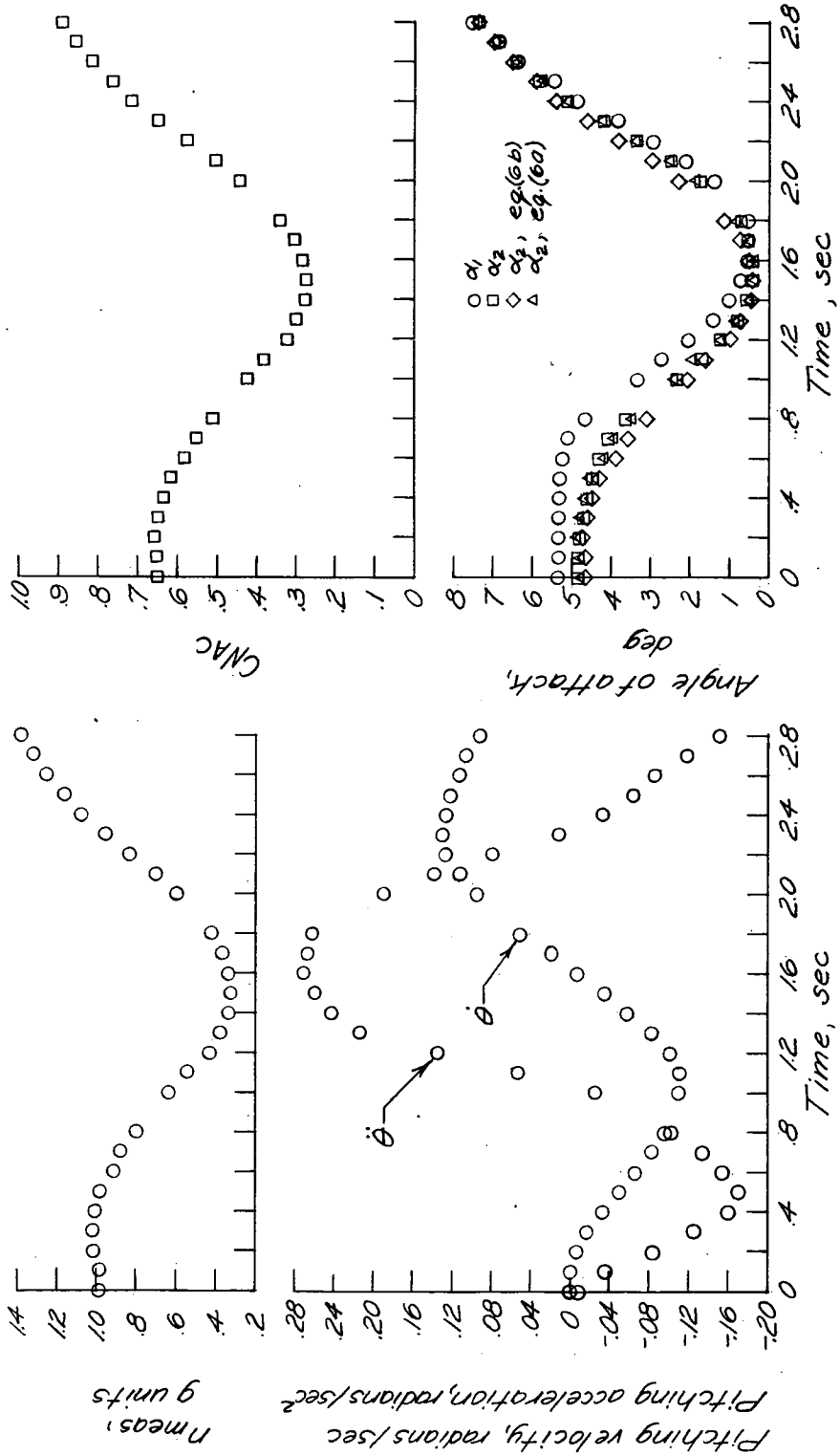

Figure 4.- Time histories of measured and calculated quantities for flight 12, run 6.

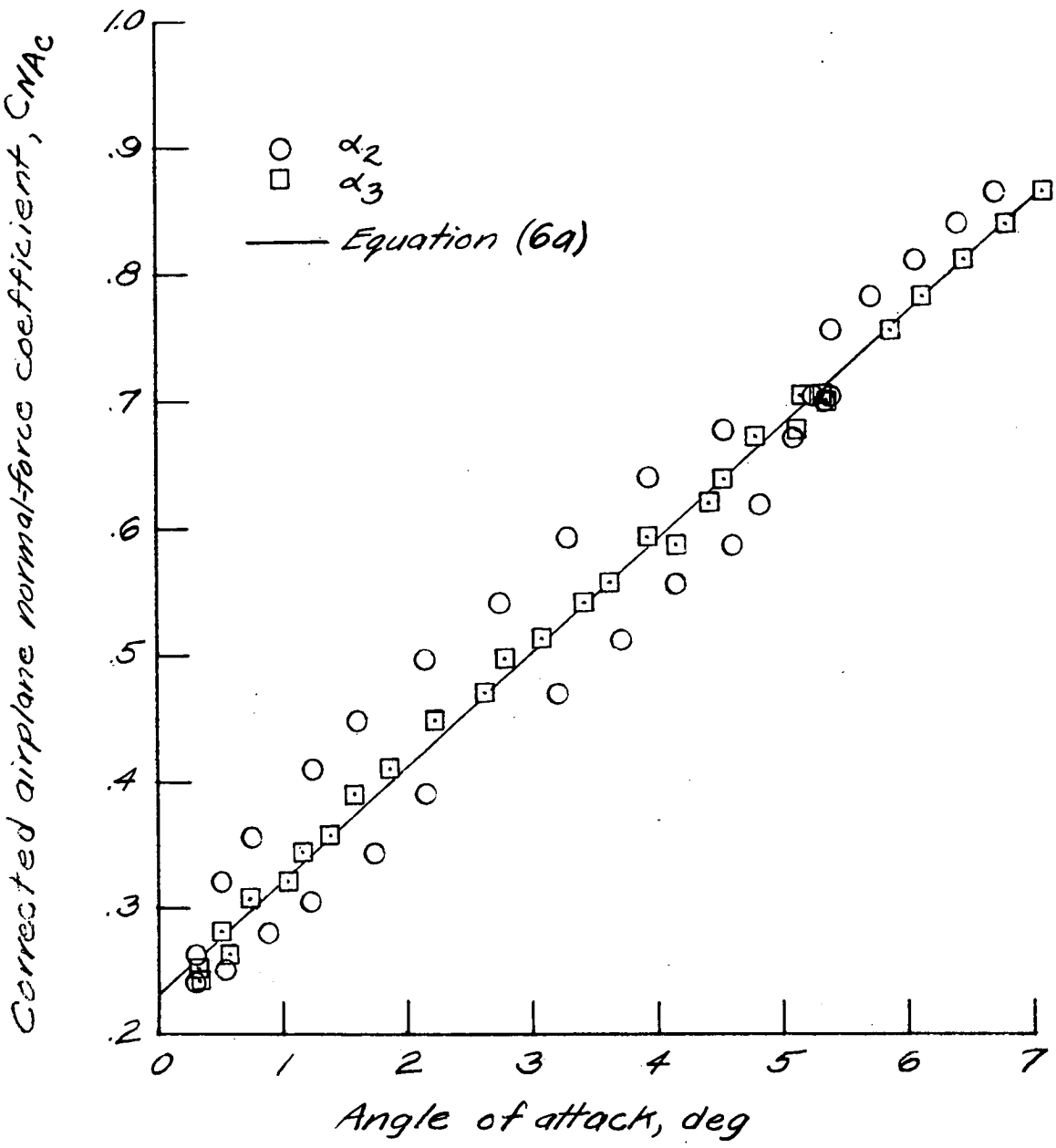

Figure 5.- Variation of corrected airplane normal-force coefficient with angle of attack α_2 and angle of attack corrected for lag α_3 for data of figure 3.

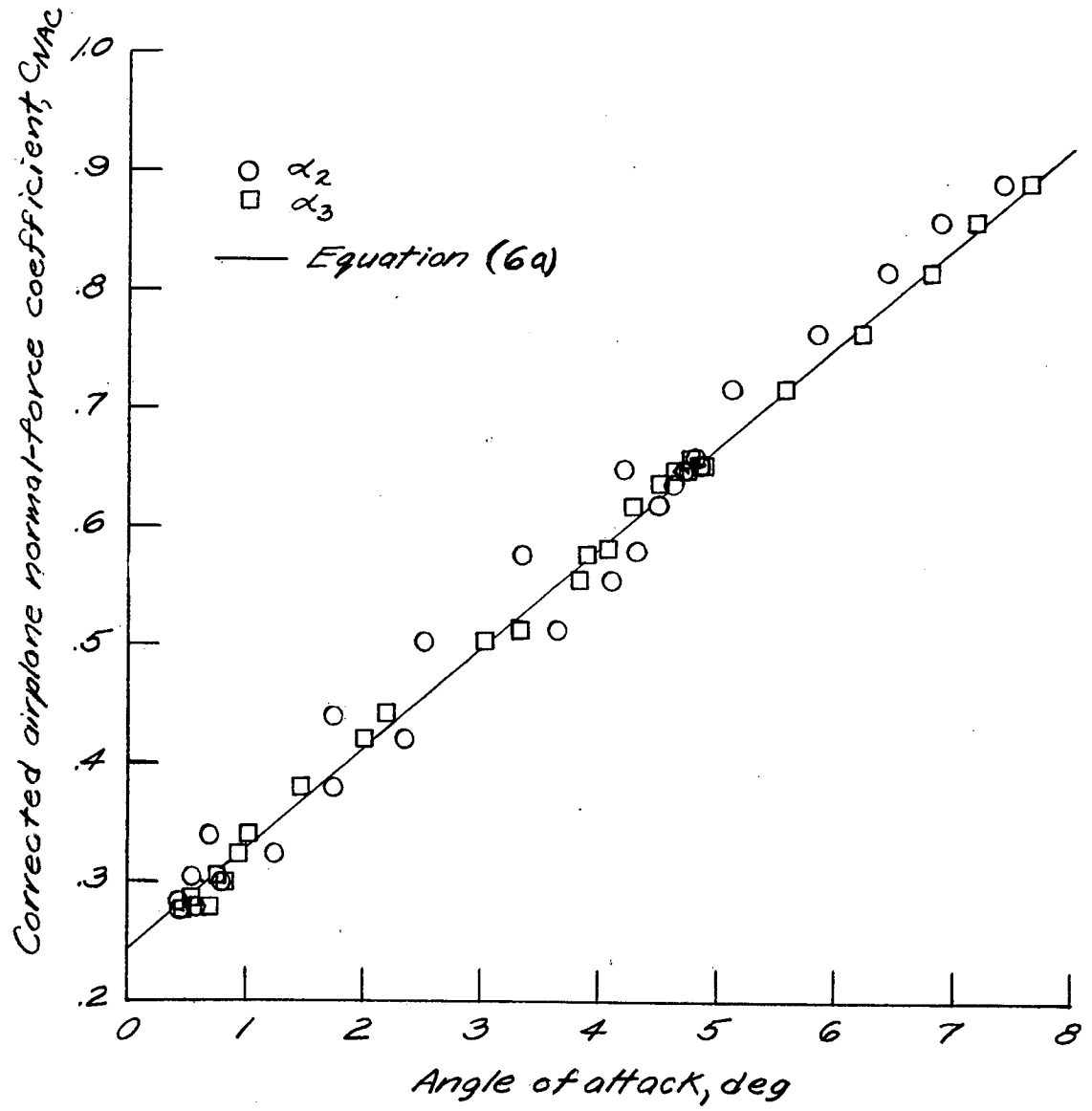

Figure 6.- Variation of corrected airplane normal-force coefficient with angle of attack α_2 and angle of attack corrected for lag α_3 for data of figure 4.

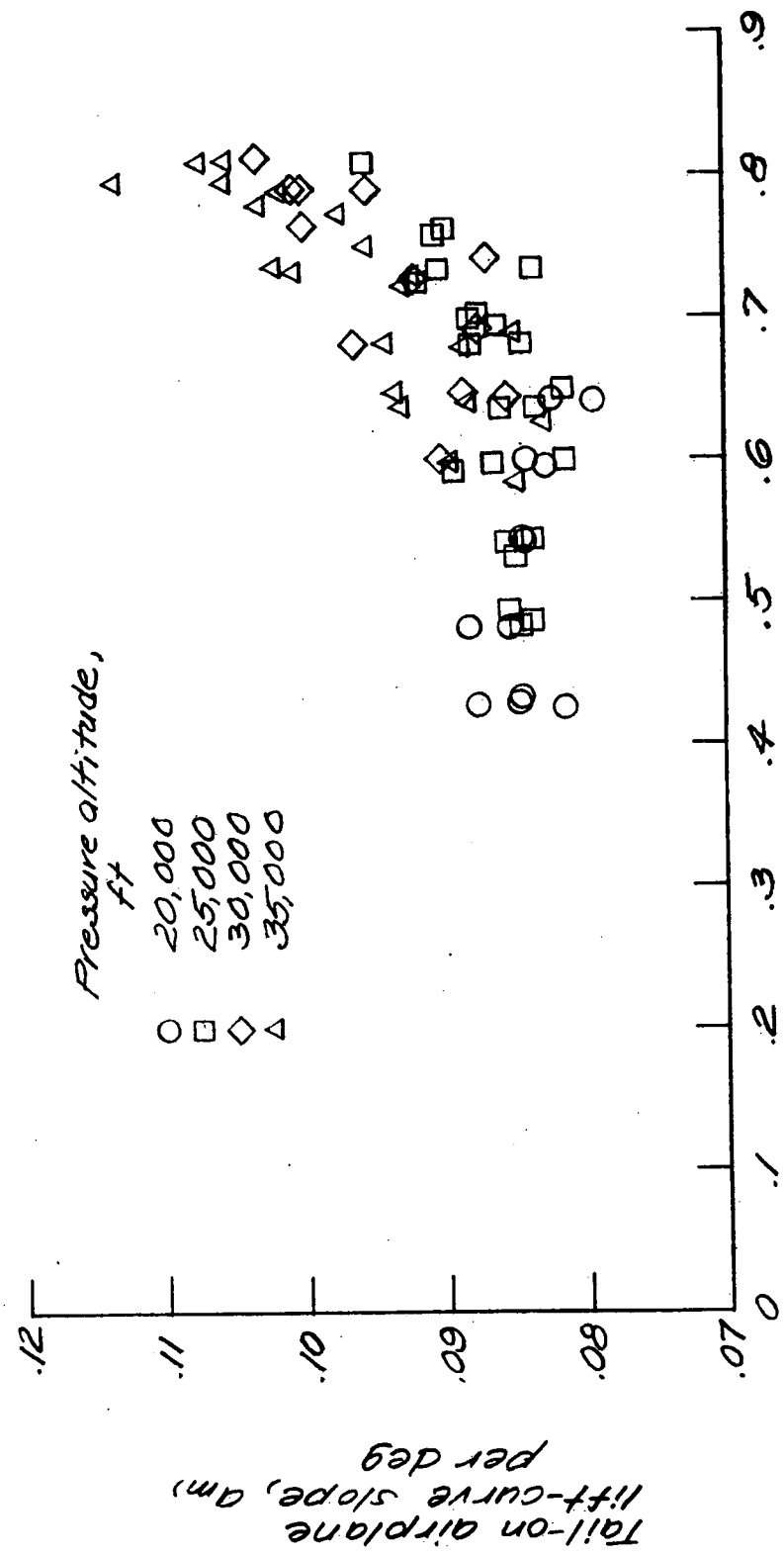

Figure 7.- Airplane lift-curve slope as a function of Mach number and altitude.

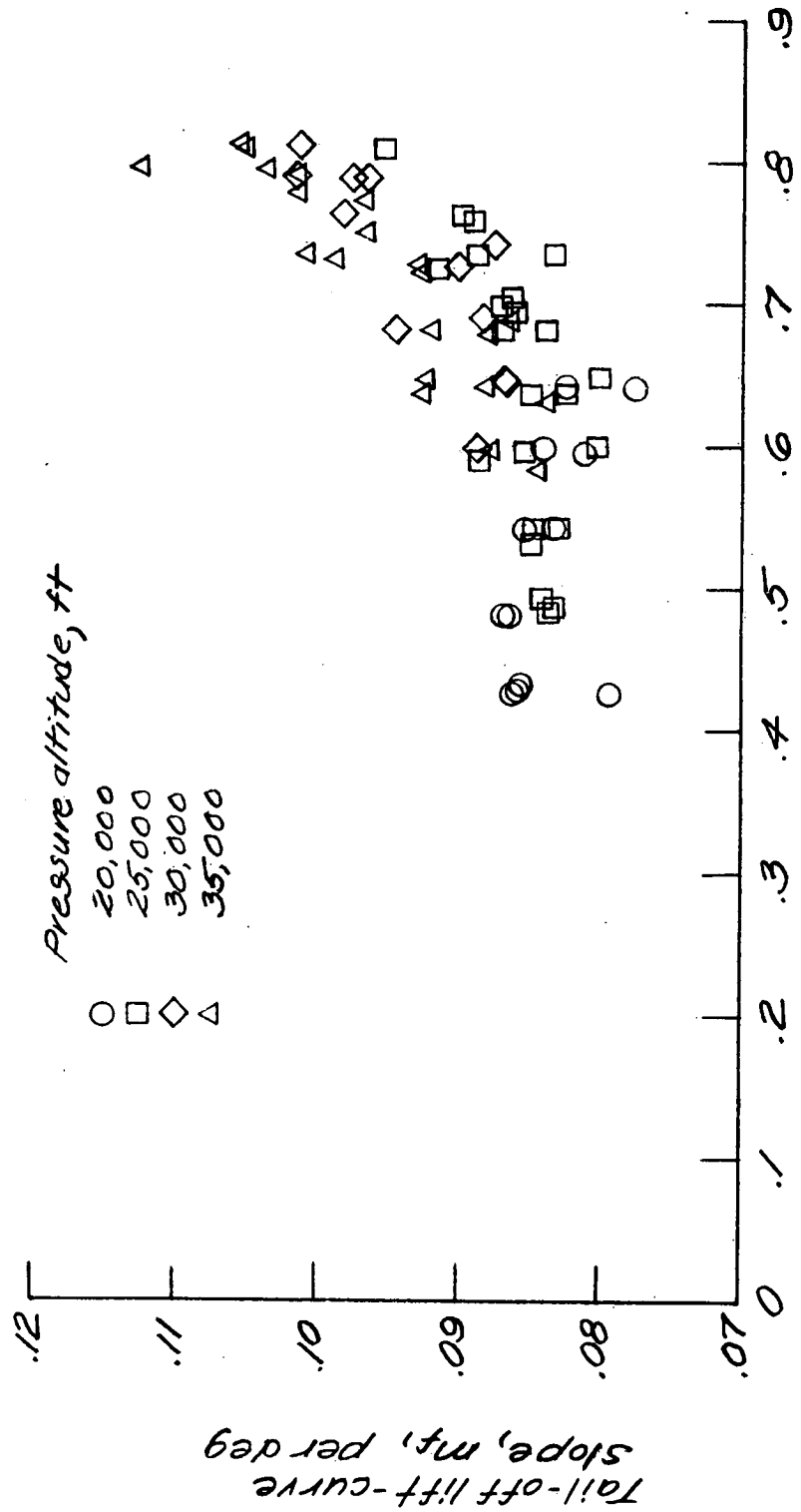

Figure 8.- Tail-off lift-curve slope as a function of Mach number and altitude.

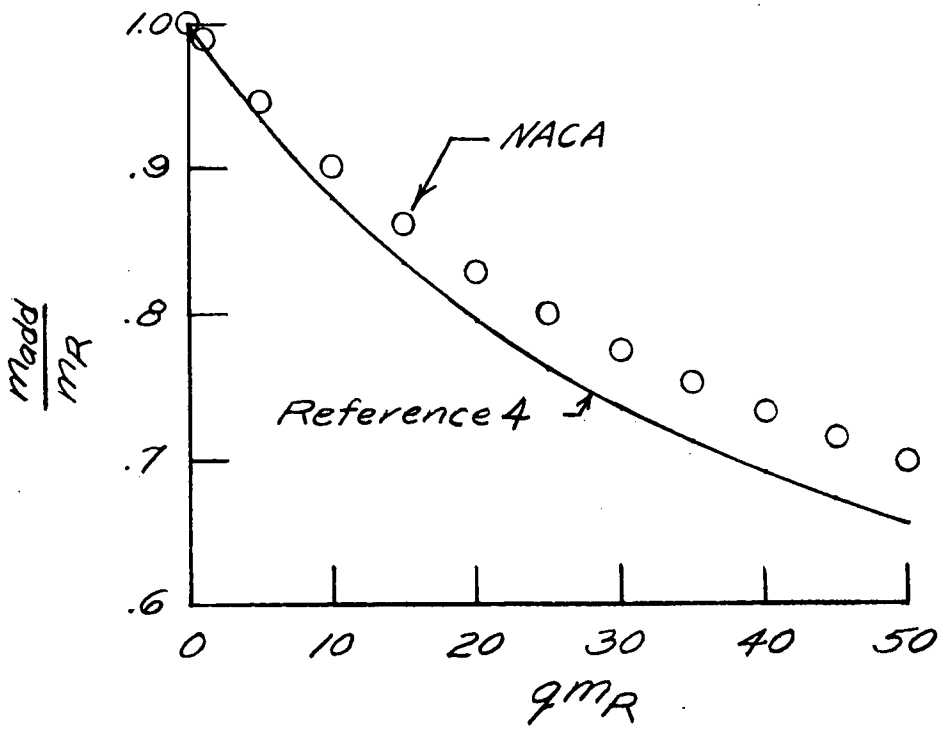

Figure 9.- Lift-curve-slope ratio as a function of flexibility parameter.

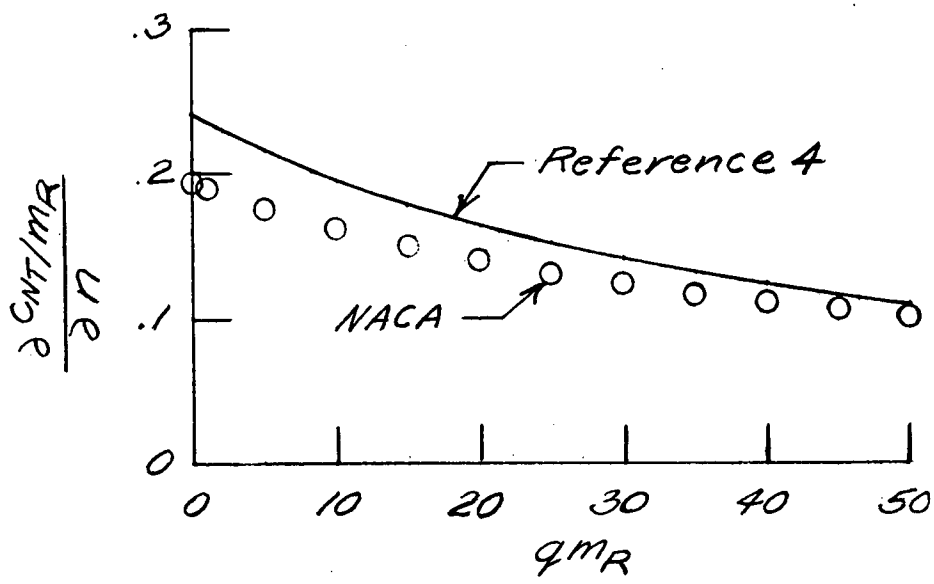

Figure 10.- Inertia flexibility parameter as a function of flexibility parameter.

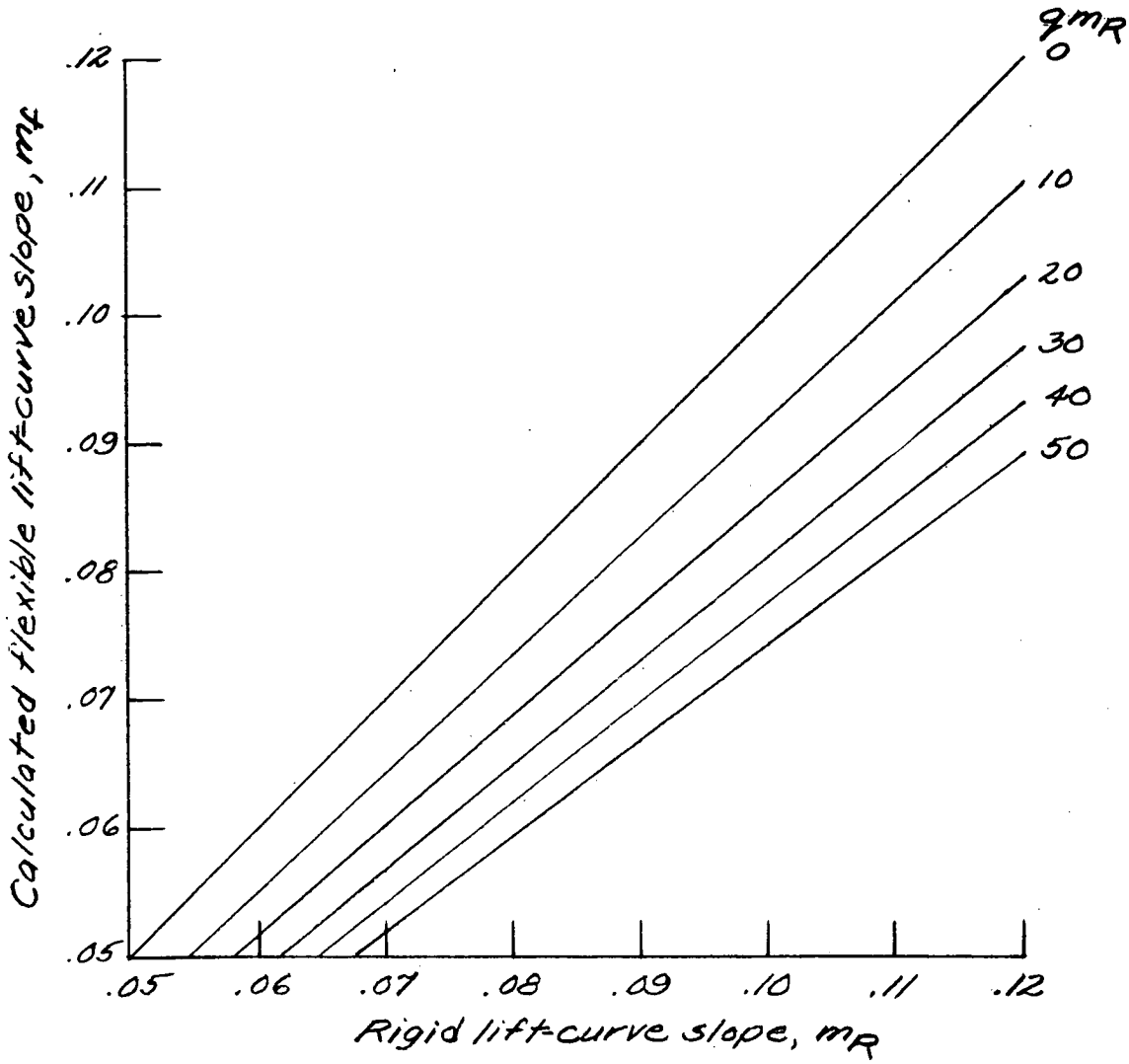

Figure 11.- Flexible lift-curve slope as a function of m_R and qm_R.

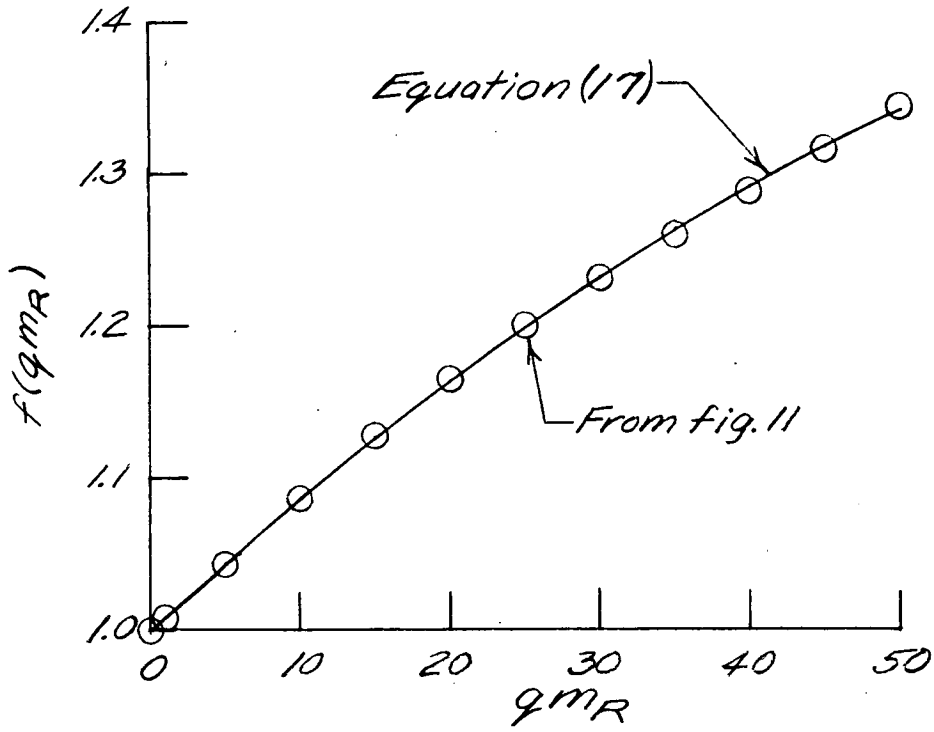

Figure 12.- Lift-curve-slope ratio $f(qm_R) = m_R/m_f$ as a function of flexibility parameter.

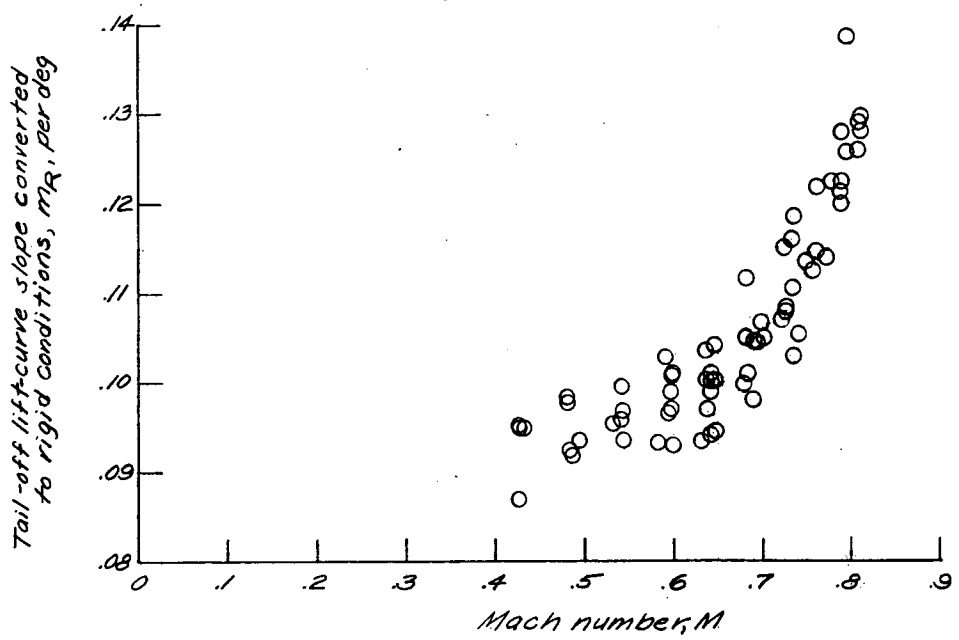

Figure 13.- Flight values of tail-off lift-curve slopes converted to rigid conditions $\left(qm_R = 0\right)$.

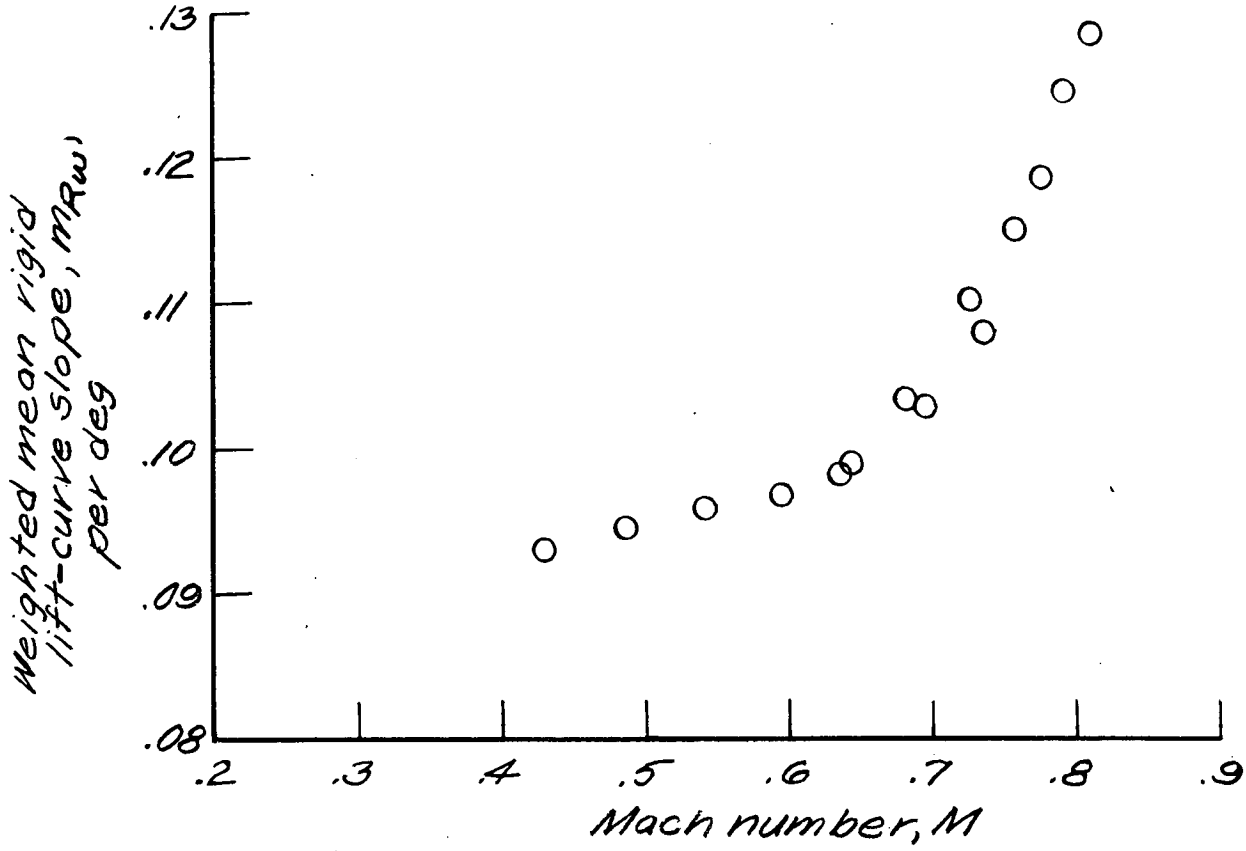

(a) Weighted mean rigid lift-curve slopes.

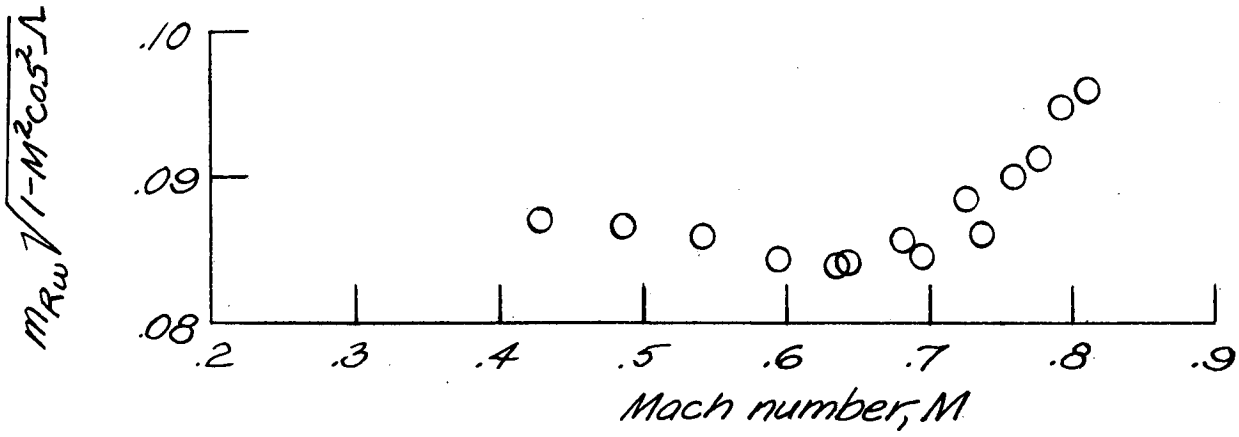

(b) Equivalent zero Mach number values of weighted mean lift-curve slopes.

Figure 14.- Weighted lift-curve slopes as a function of Mach number.

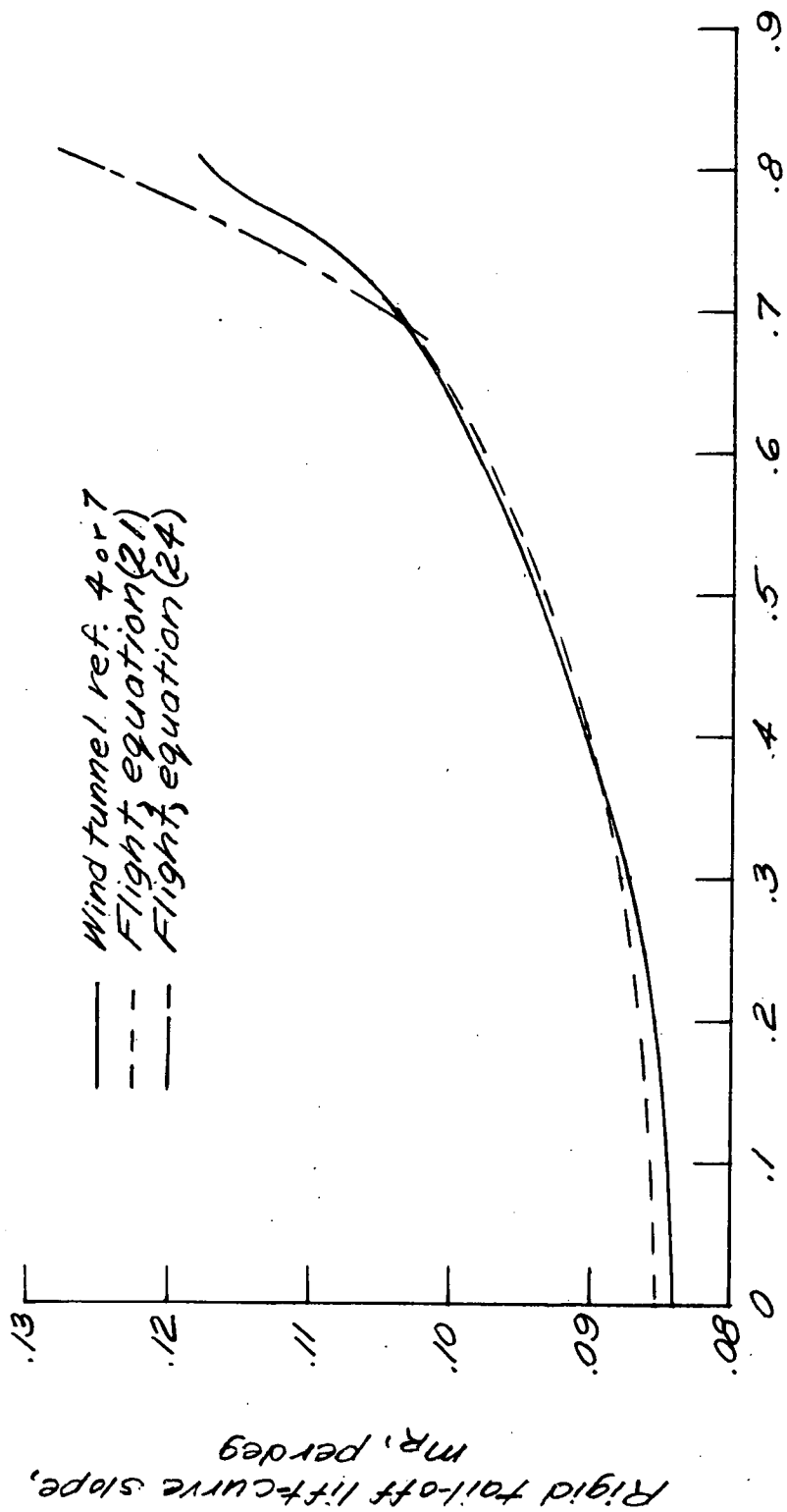

Figure 15.- Comparison of wind-tunnel rigid model and flight-test rigid tail-off lift-curve slopes.

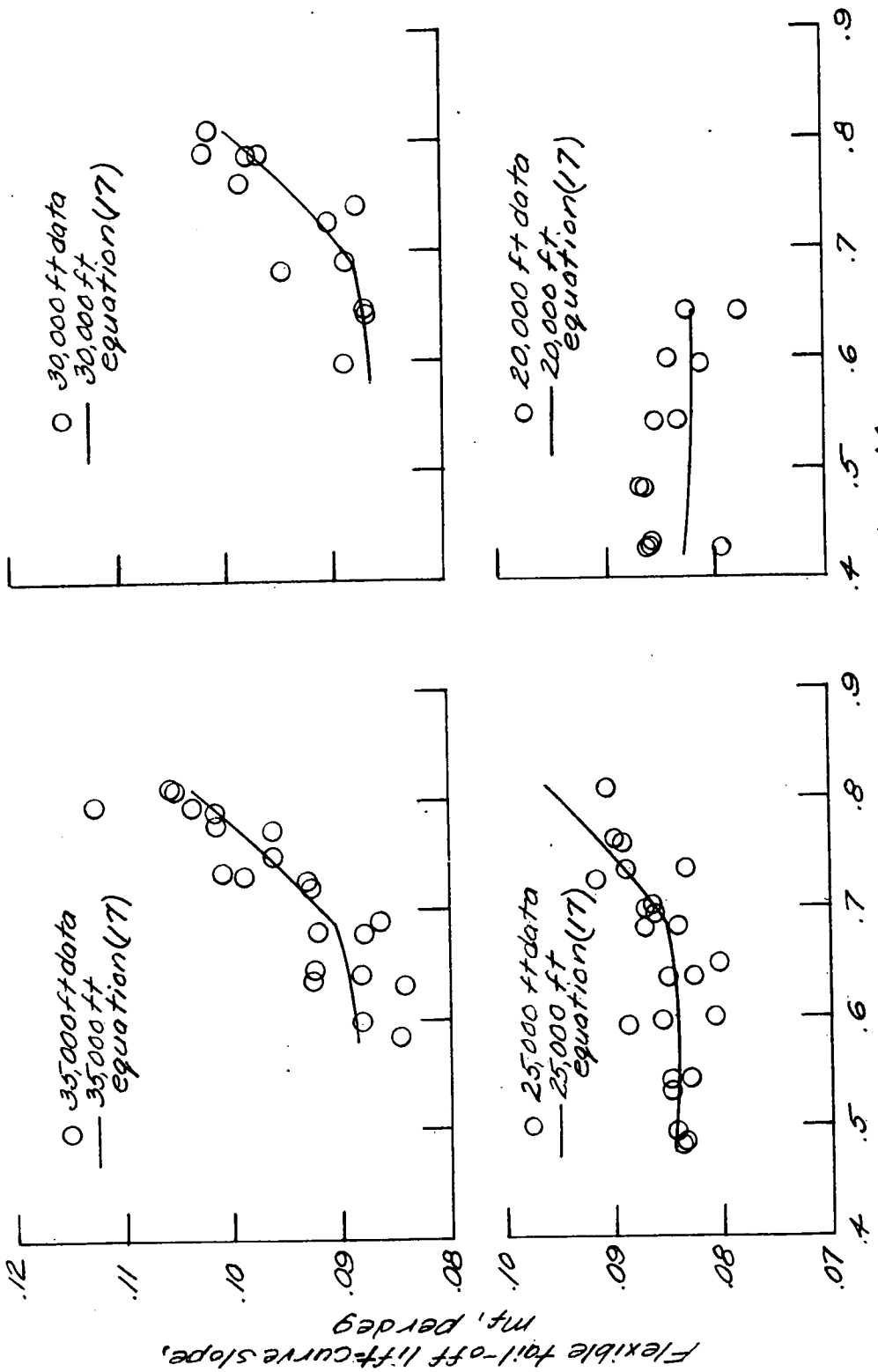

Figure 16.- Comparison of measured and calculated lift-curve slopes at test altitudes.

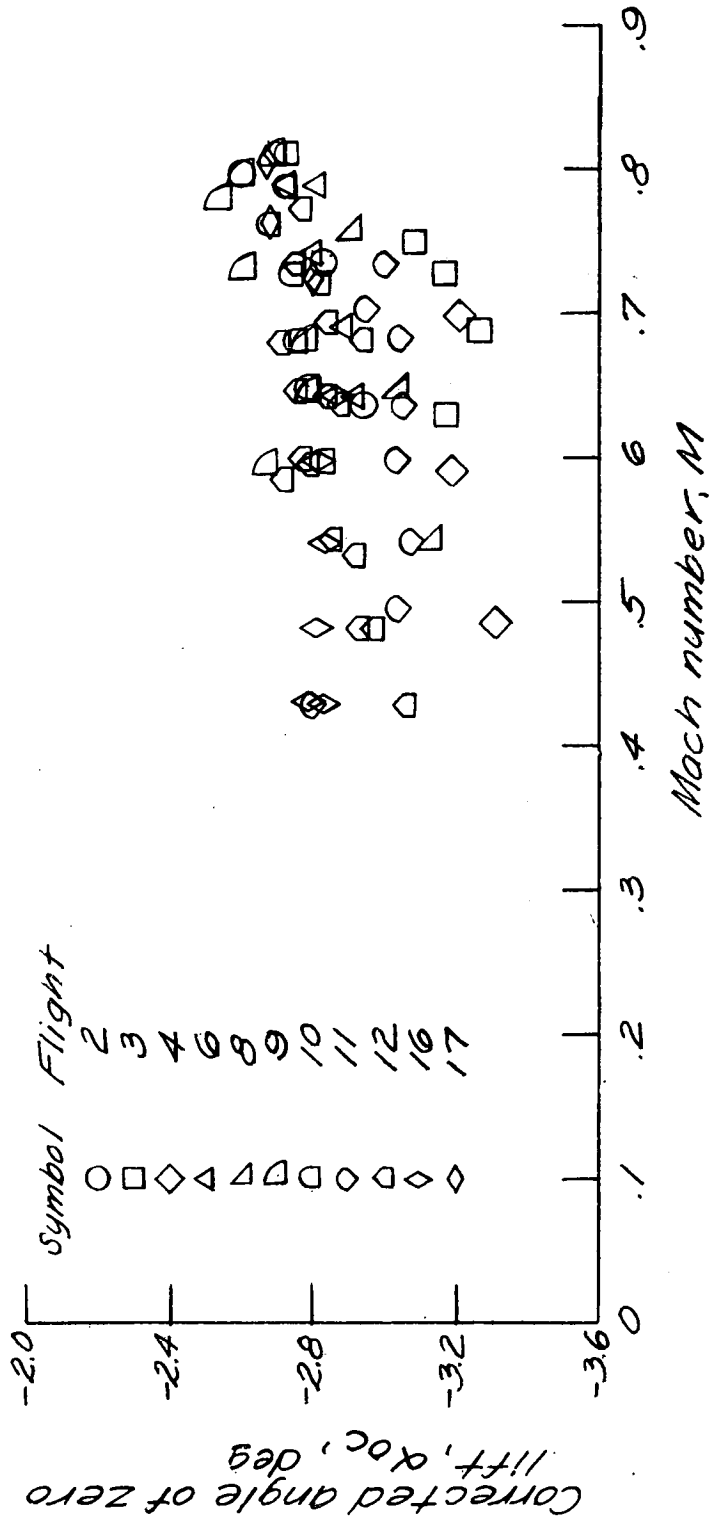

Figure 17.- Corrected angles of zero lift by flights.

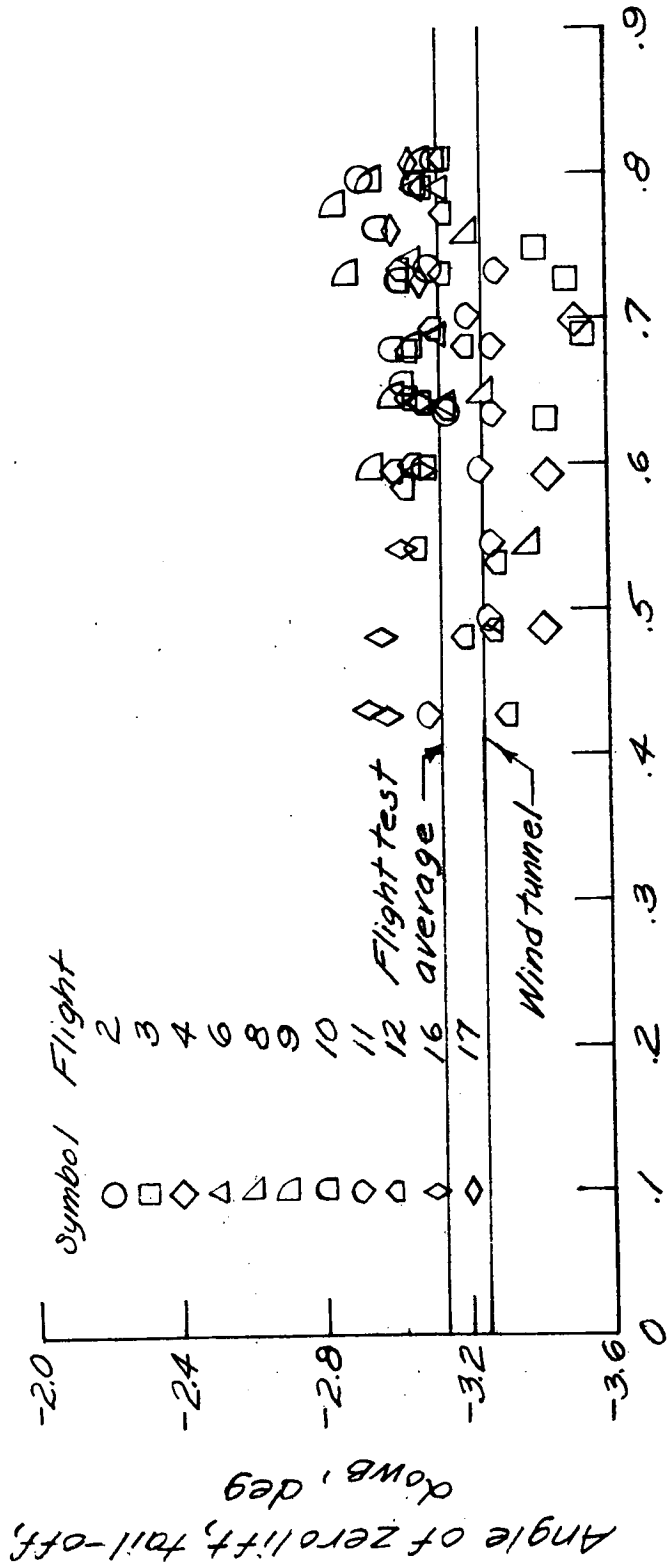

Figure 18.- Tail-off angles of zero lift by flights.

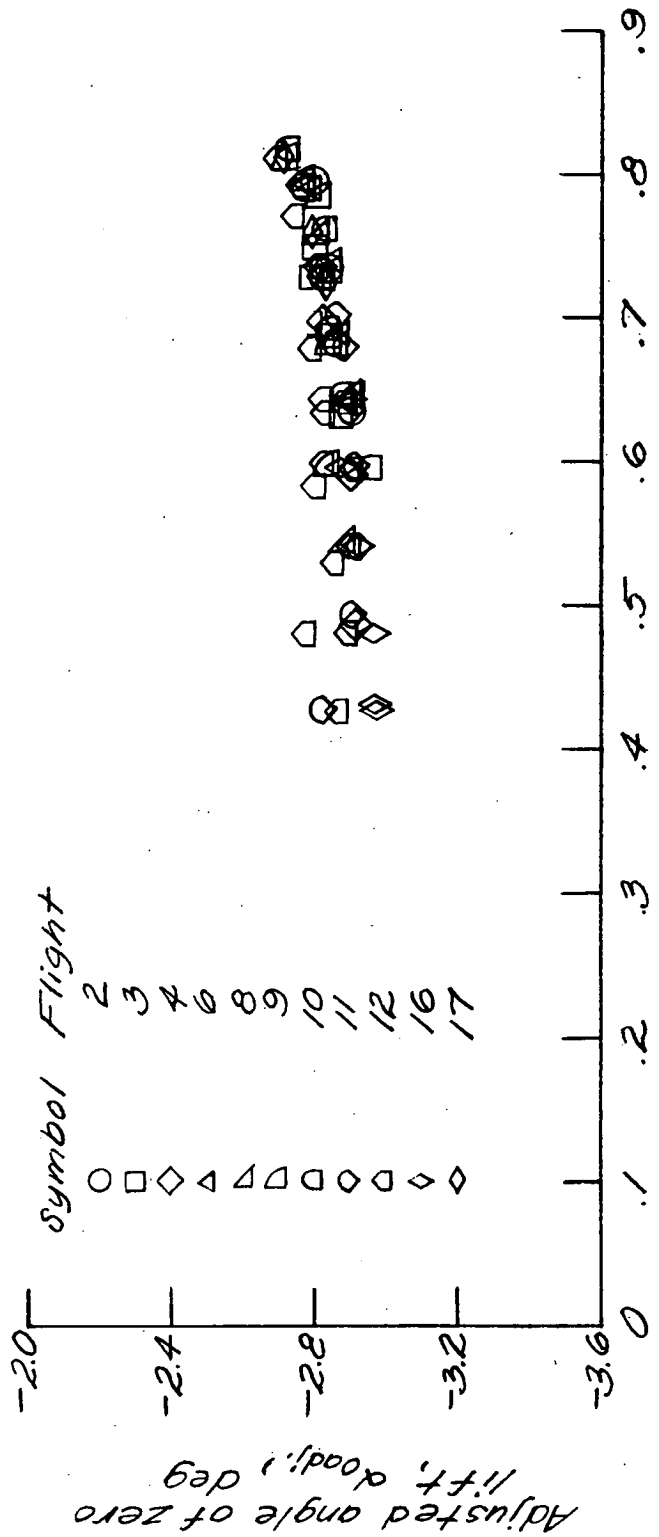

Figure 19.- Tail-on angles of zero lift adjusted for zero shifts as a function of Mach number.